Influence of circular RNA topology on Target RNA-Directed MicroRNA Degradation

Federico Fuchs Wightman[1, 2*], Jerónimo Lukin[3, 4*], Sebastián Giusti[3], Michael Soutschek[5, 6], Laureano Bragado[1, 2], Berta Pozzi[1, 2, 7], Paula González[8], Juan P. Fededa[8], Gerhard Schratt[5, 6], Rina Fujiwara[9], Jeremy E. Wilusz[9], Damián Refojo[3#] & Manuel de la Mata[2, 10#]

[1]Universidad de Buenos Aires, Facultad de Ciencias Exactas y Naturales.

[2]CONICET-Universidad de Buenos Aires, Instituto de Fisiología, Biología Molecular y Neurociencias (IFIBYNE), Buenos Aires, Argentina.

[3]Instituto de Investigación en Biomedicina de Buenos Aires (IBioBA) - CONICET - Partner Institute of the Max Planck Society, Godoy Cruz 2390, C1425FQD Buenos Aires, Argentina.

[4]Present address: Icahn School of Medicine at Mount Sinai, New York, NY, USA.

[5]Lab of Systems Neuroscience, D-HEST Institute for Neuroscience, ETH Zürich, Switzerland.

[6]Neuroscience Center Zurich, ETH Zurich and University of Zurich, Switzerland.

[7]Previous address: Institute of Cell Biology, University of Bern, Bern, Switzerland.

[8]Instituto de Investigaciones Biotecnológicas "Dr. Rodolfo A. Ugalde", IIB-UNSAM, IIBIO-CONICET, Universidad Nacional de San Martín, Buenos Aires, Argentina.

[9]Verna and Marrs McLean Department of Biochemistry and Molecular Biology, Therapeutic Innovation Center, Baylor College of Medicine, Houston, Texas, USA.

[10]Universidad de Buenos Aires, Facultad de Ciencias Exactas y Naturales. Departamento de Fisiología, Biología Molecular y Celular.

[*]Contributed equally.

[#]Correspondence: drefojo@ibioba-mpsp-conicet.gov.ar, mmata@fbmc.fcen.uba.ar.

Abstract

A subset of circular RNAs (circRNAs) and linear RNAs have been proposed to “sponge” or block microRNA activity. Additionally, certain RNAs induce microRNA destruction through the process of

Target RNA-Directed MicroRNA Degradation (TDMD), but whether both linear and circular transcripts are equivalent in driving TDMD is unknown. Here we show that RNA topology significantly influences TDMD. Consistent with previous knowledge that *Cdr1as (ciRS-7)* circular RNA protects miR-7 from Cyrano-mediated TDMD, we demonstrate that depletion of *Cdr1as* reduces miR-7 abundance. In contrast, overexpression of an artificial linear version of *Cdr1as* drives miR-7 degradation. Using plasmids that express a circRNA with minimal co-expressed cognate linear RNA, we show differential effects on TDMD that cannot be attributed to the nucleotide sequence, as the TDMD properties of a sequence often differ between its circular and linear forms. By analysing RNA sequencing data of a neuron differentiation system, we further detect potential effects of circRNAs on microRNA stability. Our results support a model in which circRNAs have a topology-dependent effect on TDMD, either avoiding or triggering it on specific microRNAs.

Keywords: circRNA/microRNA/TDMD

Introduction

Circular RNAs (circRNAs) are long known regulatory RNAs that have gained increasing attention since the first reports that highlighted their high diversity and abundance (Memczak *et al*, 2013; Hansen *et al*, 2013; Salzman *et al*, 2013; Jeck *et al*, 2013). CircRNAs are covalently closed structures that originate from pre-mRNA backsplicing and therefore lack a poly-A tail and 5'-cap. As these terminal modifications are the entry points for the microRNA (miRNA) effector machinery (Bartel, 2018; Jonas & Izaurralde, 2015), circRNAs seem largely immune to posttranscriptional degradation by miRNAs. Current knowledge points towards a diversity of both nuclear and cytoplasmic functions for different individual circRNAs, and several findings have suggested that some circRNAs regulate gene expression by working as miRNA "sponges" (Chen, 2020; Xiao *et al*, 2020; Hanan *et al*, 2020).

Whether circRNAs act on miRNAs by blocking their ability to bind linear mRNA targets, affecting their stability, or a combination of both remains to be determined. In particular, it is unclear whether some circRNAs are active in driving Target Directed MicroRNA Degradation (TDMD), a mechanism that has emerged as central in affecting miRNA turnover (Ameres *et al*, 2010; Cazalla *et al*, 2010; Marcinowski *et al*, 2012; Li *et al*, 2021b; Fuchs Wightman *et al*, 2018). During TDMD, targets with

57 extensive base-pair complementarity towards the 3′ end of the miRNA –i.e. displaying no more than 3
58 mismatches in addition to a central bulge– lead to miRNA degradation, reversing the logic of
59 canonical miRNA target silencing in which the target RNA is degraded. TDMD induces a
60 conformational change on Argonaute (AGO) proteins that leads to their poly-ubiquitination and
61 degradation, rendering the loaded miRNAs unprotected and susceptible to degradation by general
62 nucleases (Shi *et al*, 2020; Han *et al*, 2020). Unlike sponging, TDMD-inducing targets act catalytically
63 even at sub-stoichiometric levels, resulting in the most selective and potent miRNA degradation
64 mechanism described to date. This phenomenon indeed seems to explain the half-lives of most
65 naturally unstable miRNAs (de la Mata *et al*, 2015; Denzler *et al*, 2016; Kleaveland *et al*, 2018; Shi *et al*,
66 2020). A priori, the circular topology of circRNAs should not represent an impediment to regulating
67 miRNAs through TDMD, and the high stability of circRNAs could even be an advantage for this activity.
68 On the other hand, previous reports have shown that extended miRNA:target basepairing *per se* is not
69 enough to trigger TDMD and that miRNA binding must also occur within a conformationally flexible
70 region of the target for TDMD to be active (Pawlica *et al*, 2016; Li *et al*, 2021b; Fuchs Wightman *et al*,
71 2018). This property could be affected by RNA topology. However, to date, no circRNA has been
72 described to drive TDMD and the only available evidence indicates that circRNAs might instead lead
73 to miRNA stabilization (Piwecka *et al*, 2017; Chen *et al*, 2019).

74 CircRNAs are typically coexpressed with their cognate linear RNAs from a common host gene.
75 However, the circRNA:linear RNA ratio occurs in different proportions, with a subset of circRNAs
76 reaching higher levels than their cognate linear isoforms (Chen, 2020; Yang *et al*, 2022; Xiao *et al*,
77 2020). To reveal insights into circRNA-specific functions and mechanisms, a plethora of publications
78 have relied on circRNA overexpression using various inverted repeat-containing vectors (Zhang *et al*,
79 2014; Conn *et al*, 2015; Liang & Wilusz, 2014; Kramer *et al*, 2015; Li *et al*, 2017, 90; Liu *et al*, 2019;
80 Guarnerio *et al*, 2019; Memczak *et al*, 2013; Hansen *et al*, 2013). Yet, the capability of plasmid-based
81 methods to overexpress exogenous circRNAs free from overlapping, "leaky" linear RNA expression
82 remains questionable. Thus, attributing any observed effects to the overexpressed circRNA while not
83 rigorously controlling for the potential role of the undesired coexpressed linear transcripts represents
84 a potential pitfall (Pamudurti *et al*, 2017; Kristensen *et al*, 2019; Dodbele *et al*, 2021; Chen, 2020; Chu *et*
85 *al*, 2021; Ho-Xuan *et al*, 2020).

86 A key remaining question in the field is whether the circular nature of circRNAs is intrinsically or
87 mechanistically linked to their molecular functions. In this study, we aimed to elucidate whether linear
88 and circular target topologies function differently to affect miRNA stability and function. We initially
89 examined the well described *Cdr1as (ciRS-7)*-miR-7-Cyrano network of noncoding RNAs, where the
90 lncRNA Cyrano destabilizes miR-7-5p through TDMD (Kleaveland *et al*, 2018). We confirmed that the
91 circRNA *Cdr1as* protects miR-7-5p (Piwecka *et al*, 2017), while expression of an artificially linear version
92 of *Cdr1as* surprisingly triggers TDMD. We found that linear *Cdr1as* is unable to rescue loss of the
93 endogenous circRNA, suggesting that the circular topology of *Cdr1as* is crucial for avoiding TDMD.
94 Using a strategy that allows expression of an artificial circRNA with limited expression of the
95 counterpart linear transcript, we show that circular and linear transcripts differ in their TDMD
96 properties. Analogous to *Cdr1as*, one of the tested artificial circular RNAs failed to induce TDMD in
97 neurons while a different artificial circRNA induced TDMD in a cell line, with their respective
98 counterpart linear RNAs each behaving differently in both cases. Our data also present the first
99 evidence that circRNAs are capable of effectively triggering TDMD. Moreover, through a
100 computational analysis, we propose that certain circRNA-miRNA interactions might lead to topology-
101 dependent effects on miRNA stability, representing a potentially active mechanism during neuron-like
102 differentiation.
103

104 # Results

105 ## Circular topology of *Cdr1as* is necessary to protect miR-7 from TDMD

106 In order to study whether circular topology plays a role in TDMD, we studied the case of the
107 *Cdr1as*-miR-7 interaction (Hansen *et al*, 2011, 2013; Memczak *et al*, 2013). To that end, we designed
108 tools to manipulate endogenous *Cdr1as* levels in rodent primary neurons (Fellmann *et al*, 2013). A
109 lentiviral vector was engineered to express a shRNAmiR (sh*Cdr1as*) against *Cdr1as* (Figure EV1A) that
110 was then transduced into primary neurons at high efficiency. *Cdr1as* was effectively knocked down
111 (Figure 1A, EV1B) and miR-7 levels were reduced (Figure 1B), which is in line with previous evidence
112 (Piwecka *et al*, 2017). *Cdr1as* therefore does not induce TDMD but instead helps stabilize this miRNA.
113 To determine whether the observed effect was dependent on the circular topology of *Cdr1as*, we
114 attempted to rescue *Cdr1as* knockdown with the expression of an artificial linear version of *Cdr1as* –

115 lin*Cdr1as*– lacking the sh*Cdr1as* target site. Interestingly, the decrease in miR-7 abundance caused by
116 the knockdown of endogenous *Cdr1as* could be neither rescued nor significantly enhanced by co-
117 expressing the linear *Cdr1as*, even though the artificial lin*Cdr1as* reached expression levels similar to
118 those of endogenous *Cdr1as* in control cells (Figure 1A-B). Remarkably, expressing lin*Cdr1as* alone –
119 without knocking down endogenous *Cdr1as*– caused a significant destabilization of miR-7 (Figure 1C-
120 D), consistent with TDMD being driven by the RNA expressed in an artificial linear topology.
121 Importantly, the linear lin*Cdr1as* did not induce significant variation in the abundance of endogenous
122 circular *Cdr1as* (Figure EV1C). To exclude the possibility that miR-7 downregulation was a
123 consequence of changes in its transcription and/or maturation upon transduction of lin*Cdr1as*, we
124 measured the abundance of its primary transcript (pri-miR-7a-1), passenger strands (miR-7a-1-3p and
125 miR-7a-2-3p) and two (2) additional control miRNAs (miR-9 and -132). Our results confirmed that the
126 guide strand miR-7-5p, but neither the primary transcript/passenger strands nor the other control
127 miRNAs, undergo degradation upon introduction of the linear version of Cdr1as (Figure 1D, EV1D).
128 This result also confirms that the reduction in miR-7 is a post-transcriptional effect occurring after
129 miRNA processing and is therefore compatible with active TDMD triggered by the linCdr1as construct
130 (Figure EV1D). Careful inspection of the miR-7 sites present in *Cdr1as* showed that some of them
131 indeed exhibit base pairing complementarity compatible with a TDMD-competent architecture
132 (Figure EV1E) (Fuchs Wightman *et al*, 2018).

133 As an orthogonal strategy to reduce *Cdr1as* levels and rule out potential off target or indirect
134 effects caused by the sh*Cdr1as*, we used CRISPR/Cas9 genome editing to mutate the splicing sites of
135 the endogenous *Cdr1as* gene (Figure EV1F). Despite an overall lower efficacy in *Cdr1as* knockdown
136 compared to the sh*Cdr1as*, we observed a similar effect on miR-7 levels, consistent with *Cdr1as* being
137 unable to induce TDMD on miR-7 and instead leading to its stabilization (Figure EV1G-H).

138 Overall, our results show that endogenous *Cdr1as* is unable to trigger TDMD on miR-7 but rather
139 stabilizes this miRNA. Nonetheless, when expressed as an artificially linear RNA, it can engage in miR-7
140 degradation through TDMD, supporting the notion that the natural circular/linear topology, and not
141 just the nucleotide sequence of a RNA target, is a crucial determinant for engaging in such type of
142 regulation.

143

144 **Addition of microRNA perfect target sites in flanking introns improves the**
145 **specificity of artificial circRNA expression from expression vectors**

146 In order to study whether the differences in efficacy of circular and linear RNAs on TDMD are a
147 general phenomenon, we sought to set up a system capable of expressing either artificial linear
148 transcripts or circRNAs of identical primary sequences (Figure 2A). Both the linear and circular RNAs
149 contain binding sites against candidate miRNAs with TDMD-competent sequence complementarity or
150 seed-mutant controls (Figure EV2A). To express the circRNA, we flanked the region to be circularized
151 with splice sites and flanking introns from a naturally circularized RNA (human ZKSCAN1 exons 2 and
152 3) that contain Alu reverse complementary sequences (RCS) that drive backsplicing (Figure 2A) (Liang
153 & Wilusz, 2014). In order to preferentially enrich the expression of the circular over the linear variant in
154 neurons, we further introduced perfectly matched sites against a highly expressed neuron-specific
155 miRNA (miR-124) in the downstream intron that is lost after production of the backspliced circular
156 product (Figure 2A). These miRNA sites remain in the linear RNA isoform, thus rendering the linear –
157 but not the circular– RNA form susceptible to AGO2 slicing. In parallel, we expressed a linear transcript
158 with identical sequence to the circRNA-expressing construct, but lacking the splice sites and flanking
159 introns that induce circularization (Liang & Wilusz, 2014) (Figures 2A and EV2A). The latter constructs
160 have proved effective in triggering TDMD in primary neurons (de la Mata *et al*, 2015). All constructs
161 were packed into lentiviral vectors and used to transduce mouse primary neurons.

162 In order to validate that the constructs expressed a single circRNA species with covalently linked
163 ends, we performed Northern blot analysis of RNase R treated or untreated samples from HEK293T
164 transfected cells –a cell line where miR-124 is not endogenously expressed (Figure EV2B). We
165 observed that circRNA-expressing constructs bearing either perfect or seed-mutant sites for miR-124
166 produced two bands: an RNase R-resistant circRNA and an RNase R-sensitive linear RNA form. This
167 result confirms the circular topology for the artificially expressed circRNA (Figure EV2B and D).
168 Importantly, quantification of northern blot bands correlated well with RT-qPCR measurements using
169 primers that detected the circular isoform exclusively (Figure 2A, primer pair #1) or both the linear and
170 circular isoforms combined –hereafter referred to as Total Output (TO)– (Figure 2A, primer pair #2),
171 further validating the latter method for subsequent analysis (Figure EV2C). We confirmed usage of the
172 appropriate back-splicing junction with two reverse transcriptase enzymes (MMLV-RT and Superscript

173 II), thereby further ruling out the likelihood of artifacts due to template switching during cDNA
174 synthesis (Figure EV2E).

175 To validate that our strategy was successful at expressing a circRNA while selectively degrading its
176 counterpart linear transcript by means of miR-124, we transduced the circRNA-expressing constructs
177 into mouse primary neurons. We observed a potent (3-4 fold) degradation of "leak" linear RNA
178 without affecting circRNA abundance (Figure 2B). Furthermore, circRNAs were produced exclusively
179 from the circRNA-expressing construct and not from the linear RNA-expressing construct (TDMD
180 inducer), while both constructs produced equivalent total output levels (Figure 2C). A similar result
181 was observed in HEK293T cells when the miR-124 sites were replaced with a perfect match against
182 miR-92a, a highly expressed miRNA in this cell line. Under these conditions, a 2-fold reduction of the
183 linear RNA was observed without affecting circRNA levels (Figure EV2F). Altogether, these results
184 confirm that our system is effective in expressing circRNAs while reducing the abundance of their
185 cognate linear RNAs, making it a generally useful tool in experiments aimed at dissecting circRNA
186 function.

187

188 **CircRNA-expressing constructs reveal topology-dependent effects on TDMD**

189 Using the constructs described above, we next explored whether linear and circular target
190 topologies differently affect miRNA stability through TDMD in neurons, a cell type with potent TDMD
191 activity (de la Mata *et al*, 2015). To this end, we transduced primary neurons with either linear or
192 circRNA expression constructs bearing TDMD-competent (bulged) or seed-mutant binding sites
193 against miR-132. The linear TDMD inducer was capable of effectively destabilizing miR-132, but the
194 circRNA-expressing construct showed no effect on miRNA stability (Figure 3A) even when both
195 constructs were expressed at similar overall levels (Figure 2C). Based on the performance of the
196 circRNA-expressing construct in neurons (i.e. 3-4 fold specific reduction of linear RNA by-products and
197 similar total transcript levels), we estimate that circRNA levels account for up to 30-50% of the total
198 RNA expressed (compared to the ca. 25% in HEK293T cells with no endogenous miR-124). With this
199 technical limitation in mind, we conclude that the artificial circRNA appears unable to contribute to
200 TDMD and may even antagonize the TDMD effect driven by its co-expressed linear counterpart
201 (Figures 2C and 3A). We confirmed that miR-132 downregulation by the linear TDMD inducer was not

202 a consequence of changes in transcription and/or maturation of the targeted miRNA by showing that
203 the abundance of the primary transcript (pri-miR-132) and passenger strand (miR-132-5p) of miR-132
204 remained unchanged (Figure EV3A). The reduction of the miR-132 guide strand was thus a bona fide
205 post-transcriptional effect occurring after miR-132 processing and is therefore consistent with TDMD.
206 We further examined the specificity of the linear TDMD inducer and confirmed that the levels of four
207 additional unrelated mature miRNAs (miR-124, -128, -138 and -409) were not significantly affected
208 (Figure EV3A).

209 Since the lack of TDMD could be attributed to the inability of the circular RNA to bind to the RISC
210 complex, we performed an RNA immunoprecipitation experiment (RIP) by specifically pulling-down
211 AGO2 and isolating all copurifying RNA species. We co-transfected HEK293T cells with FLAG/HA-
212 AGO2, the different circRNA-expressing constructs and a vector for pri-miR-132 (otherwise absent in
213 HEK293T cells), followed by anti-FLAG RIP and RT-qPCR analysis. The artificial circRNA was effectively
214 pulled down with AGO2 when carrying bulged sites for miR-132, but not when the sites were mutated
215 at the miRNA seed-binding region (Figures 3B and EV3B-C). This thus demonstrated that the circular
216 RNA is indeed able to specifically bind to the RISC complex.

217 We next reasoned that the observed differences could be the trivial consequence of differential
218 localization of the circRNA relative to the linear isoform. To exclude this possibility, we performed
219 subcellular fractionation and observed that the artificial circRNA accumulated in the cytoplasm at
220 similar proportions relative to the linear control, with the former being only slightly lower in the
221 nuclear compartment (Figures 3C and EV3D-E). We conclude that the inability of the circRNA to trigger
222 TDMD is not related to it being retained in the nucleus.

223 The behaviour observed for the circRNA tested up to this point led us to ask whether avoiding
224 TDMD was a general phenomenon. To answer this, we generated additional constructs that express
225 circRNAs of different sizes from a different backbone based on *Drosophila laccase2* introns which have
226 been previously shown to produce high levels of circRNAs (Kramer *et al*, 2015) (Figure 4A). Following a
227 similar approach as described above (Figure 2A), we introduced a perfectly matched site in the
228 downstream intron against a highly expressed miRNA in HEK293T cells (miR-92a) in order to
229 selectively degrade the linear RNA isoform that can be co-expressed from the vector. In parallel, we
230 also generated the corresponding linear RNA-expressing controls. Within both the circularized region

231 and linear RNAs, we introduced TDMD-competent (bulged) or seed-mutant binding sites against miR-
232 218, a miRNA of low/intermediate endogenous expression in HEK293T cells. Due to the presence of a
233 segment from the poly A signal, the linear RNAs are expected to be slightly longer than their circular
234 equivalents.

235 When transfected into HEK293T cells, the respective constructs conveniently produced essentially
236 only circular or linear RNAs (Figures 4B and EV4A). The different gel migration patterns observed were
237 consistent with differences in both topology and size, with the linear RNA consisting of a slightly
238 longer sequence due to the polyadenylation signal and the poly-A tail. Remarkably, while both
239 circular and linear long RNAs (1408 and ca. 1570 nt respectively) induced miR-218 degradation, only
240 the circular –but not the linear– short RNA (367 and ca. 480 nt respectively) induced TDMD (Figure 4C).
241 Importantly, neither construct significantly affected the primary transcripts of miR-218 (pri-miR-218-1
242 and -2) nor an unrelated miRNA (miR-9-5p), consistent with a post-transcriptional TDMD effect of the
243 construct acting on miR-218 (Figure EV4B).

244 Overall, this result was in clear contrast to the previous one shown in neurons, where only the
245 linear RNA –but not the circular RNA– induced TDMD (Figure 3). Nevertheless, despite the different
246 effect directions observed for the circRNA-miRNA pairs in the different cell types, our results strongly
247 favour the idea that target RNA topology influences TDMD efficacy.

248

249 CircRNAs potentially stabilize dozens of microRNAs across neuron-like 250 differentiation

251 Based on our results, we hypothesized that circRNAs might possess the ability to influence miRNA
252 stability by either driving or evading TDMD. Yet, whether this type of regulation could be a
253 widespread phenomenon was unclear. To explore this possibility, we analysed available sequencing
254 data of miRNA, circRNA and mRNA expression from hESC H9 cells in the undifferentiated state as well
255 as when they have differentiated into forebrain (FB) neuron progenitor cells (Chen *et al*, 2015; Zhang
256 *et al*, 2016). A significant proportion of circRNAs are known to be regulated along neuron
257 differentiation –with upregulation being more frequent than downregulation (You *et al*, 2015; Rybak-
258 Wolf *et al*, 2015). Concomitantly, neuron-specific miRNAs are known to become more susceptible to
259 degradation in more mature neurons (Krol *et al*, 2010), thus enabling a potential scenario in which

260 circRNAs act by selectively regulating miRNA stability. In order to consider only biochemically
261 supported circRNA-miRNA interactions, we used CLIP-Seq experimentally supported mRNA-miRNA,
262 lncRNA-miRNA and circRNA-miRNA interaction networks catalogued in the STARBASE v3/ENCORI
263 database (Yang *et al*, 2011; Li *et al*, 2014) as a proxy for bona fide interactions.

264 We first analyzed whether the abundance of specific miRNAs across the neuron-like differentiation
265 process was dependent on the extent of pairing offered by circRNAs. To this end, we initially
266 computed the total number of specific miRNA sites contributed by all circRNAs weighed by circRNA
267 levels before differentiation (hereafter referred to as "miRNA-specific effective sites" on circRNAs, see
268 materials and methods and Dataset EV1). We observed that miRNA fold changes across differentiation
269 show no apparent correlation with the number of miRNA-specific effective sites on all circRNAs (Figure
270 5A). To then obtain a stoichiometrically relevant estimate of the relative circRNA pairing to which each
271 miRNA is subjected at the onset of differentiation, we further weighted the miRNA-specific effective
272 sites to each miRNA's abundance before differentiation (Figure 5B, ranked in Dataset EV1). According
273 to this analysis, the most highly paired miRNAs, corresponding to those potentially interacting with
274 multiple and/or highly expressed circRNAs, are significantly upregulated across differentiation relative
275 to the least paired miRNAs (Figure 5B-C).

276 We next searched for additional evidence in support of a stabilizing effect of circRNAs which could
277 account for the observed differences in mature miRNA fold changes across quartiles of increasing
278 relative pairing to circRNAs. We estimated changes in pri-miRNA abundance as a proxy for changes in
279 transcription levels of the respective miRNAs across differentiation. Interestingly, while we observed a
280 positive correlation between mature miRNA and pri-miRNA fold changes, the correlation became
281 weaker for the most highly paired miRNAs (Figure 5D). By fitting the data to a multiple regression
282 model with interaction, we found that the fold change in mature miRNA levels for the more highly
283 paired miRNAs (quartile "+++ paired") seems differentially dependent on the fold change of pri-
284 miRNA levels relative to the least paired miRNAs (quartile paired) (i.e., the slope changes by ≈2 fold, p-
285 value for the interaction term = 0.0354) (Figure 5D). While this analysis showed that changes in mature
286 miRNA levels are to a large extent explained by changes in transcription of their host genes, the
287 impaired correlation and difference in slope observed for miRNAs in the most highly paired quartile
288 are consistent with an effect on stability that cannot be solely explained by changes in their

289 transcription rates. In sum, although we cannot rule out the possibility that the more highly
290 upregulated miRNAs are more efficiently processed from their pri-miRNAs than the less upregulated
291 ones, our analysis argues for a post-transcriptional effect of circRNAs on miRNA stability acting in
292 parallel to –but independently of– changes in miRNA transcription. This effect may occur through the
293 concerted interaction of individual miRNAs with highly expressed circRNAs (one or multiple) across
294 differentiation.

295 We next followed a complementary approach from a circRNA perspective, asking whether the
296 extent of pairing offered by each circRNA, namely their ability to simultaneously interact with different
297 miRNAs across differentiation, could impact their own abundance. To that end, we calculated a
298 "circRNA-specific pairing capacity" index of each individual circRNA based on the total number of sites
299 (for all miRNAs) present on the circRNA weighed by circRNA levels before differentiation (see materials
300 and methods and Dataset EV1). We observed that an increasing "pairing capacity" index did not
301 correlate with changes in circRNA fold changes across differentiation, which is consistent with the
302 notion that circRNAs are not subjected to regulation by miRNAs (Figure 5E). The collection of miRNAs
303 and circRNAs interacting across this neuron-like differentiation process includes more than a hundred
304 miRNAs and dozens of circRNAs. In fact, by focusing on the circRNAs predicted to be most highly
305 paired, this analysis suggests that circRNAs with the highest pairing capacity for miRNAs lie at highly
306 connected nodes within a complex network, further supporting the view that some individual
307 circRNAs might act as potential scaffolds for multiple miRNAs (Figure EV5A).

308

309 Predicted binding of miRNAs to circRNAs through TDMD-like interactions

310 Previous knowledge indicates that a limiting number of bona fide TDMD sites –present even at
311 sub-stoichiometric levels– can act catalytically to outcompete the tens of thousands of canonical
312 miRNA binding sites present in the transcriptome (de la Mata *et al*, 2015; Denzler *et al*, 2016;
313 Kleaveland *et al*, 2018; Shi *et al*, 2020). This might seem at odds with our results indicating those TDMD
314 sites can be either antagonized or outcompeted by a few thousand binding sites present on a subset
315 of circRNAs. Conceivably, this conundrum could be explained if TDMD-like architectures were
316 enriched on circRNAs themselves. In this scenario, the ability of circRNAs to resist canonical miRNA-
317 mediated target degradation would render the TDMD-like sites present on circRNAs more effective in

318 either competing against or triggering TDMD compared to other sites present on linear RNAs. To test
319 this hypothesis, we searched for TDMD-like architectures within circRNAs (Figure EV6A) and linear
320 mRNAs using a TDMD-site prediction tool (Soutschek *et al*, 2022). Considering that most circRNAs are
321 expressed from protein coding genes (Guo *et al*, 2014), we analysed the overlapping genomic regions
322 (5'UTR, CDS, 3'UTR) of such genes only. Since most natural circRNAs are considered to be either not
323 translated or only poorly translated via low efficiency cap-independent mechanisms (Yang *et al*, 2022),
324 we assumed that they would be in principle largely available for miRNA pairing irrespective of the
325 genomic region of origin due to little interference by translating ribosomes. This was further
326 supported by the fact that we found no association between overall miRNA-pairing and the genomic
327 region circRNAs originate from (Figure EV5D). We therefore analyzed circRNAs originating from exons
328 of all genomic regions within genes. On the other hand, for linear RNAs, we considered only 3'-UTRs
329 within the corresponding protein-coding genes as those are the gene regions where most productive
330 miRNA pairing occurs. Sites in 5'-UTRs and ORFs are ineffective as miRNAs appear to quickly dissociate
331 due to displacement by the ribosome during scanning and elongation, respectively (Grimson *et al*,
332 2007; Gu *et al*, 2009). According to our analysis, the most highly paired miRNAs are predicted to
333 interact through TDMD-like interactions with both linear and circRNA at a higher proportion than the
334 least paired miRNAs, and with an overrepresented proportion of interactions on circRNAs. From this
335 analysis, we conclude that TDMD-like sites on circRNAs may be particularly effective in affecting
336 miRNA stability across differentiation (Figure 6A-B and EV6B-C).
337

338 ## Discussion

339 A largely unresolved question in the field is whether circRNA topology –i.e., their circular nature– is
340 intrinsically relevant for them to exert their molecular actions. Alternatively, circRNAs might have been
341 evolutionarily selected merely based on their resistance to exonucleases that confer them special
342 stability properties. Most experimental approaches have largely relied on knocking down or
343 overexpressing circRNAs in different organisms or cultured cells, and undesirable artifacts can
344 commonly act as confounding factors in the interpretation of the results. In particular, overexpression
345 of circRNAs often suffers from a major caveat related to the co-expression of unwanted linear RNA
346 species from commonly used expression vectors. This type of problem can easily lead to conclusions

347 where functions are wrongly assigned to circRNAs under circumstances where the associated linear
348 transcripts are the true functional molecules (Dodbele *et al*, 2021; Ho-Xuan *et al*, 2020; Chu *et al*, 2021).
349 We have attempted to address this issue by designing a strategy that allows us to express circRNAs
350 while keeping expression of the counterpart linear product to a minimum. A similar strategy was
351 previously reported in a different context with the goal of restricting expression of transgenes to
352 specific tissues (Brown *et al*, 2007). In our hands, the approach proved to work as an efficient tool to
353 deliver high levels of circRNAs while limiting the expression of the linear RNA derived from the
354 circRNA construct (Figures 2, EV2F).

355 We have exploited this tool to gain further insights into the well-known role of circRNAs in
356 affecting miRNA function. Despite being neither prevalent nor unique to circRNAs as a class, the
357 capacity to inhibit or "sponge" miRNA silencing activity has been the most extensively documented
358 function of circRNAs (Chen, 2020; Dodbele *et al*, 2021). In spite of this, a clear picture of the mechanism
359 by which some circRNAs act on miRNAs is still missing. For instance, it remains unclear whether
360 circRNAs act on miRNAs simply by blocking their function and/or by affecting their stability. It has
361 been speculated that circRNAs might trigger TDMD similarly to some linear RNAs, but this premise
362 was never formally and experimentally tested to date (Gasparini *et al*, 2020). Our data suggest that
363 circular and linear RNAs carrying identical sequences differ in their TDMD properties. This is largely
364 recapitulated by the endogenous circRNA *Cdr1as* which cannot trigger TDMD on miR-7 except when
365 artificially expressed as a linear RNA.

366 Although our results do not formally prove it, the topology effects of *Cdr1as* on miR-7 stability
367 might be explained by the properties of the *Cdr1as*-miR-7-Cyrano network. Accordingly, the
368 stabilization of miR-7 might emerge from the inability of *Cdr1as* to drive TDMD in combination with its
369 ability to bind and compete for miR-7, ultimately shielding the exceptionally potent TDMD activity
370 driven by Cyrano on miR-7 (Kleaveland *et al*, 2018). A similar reasoning might apply to the fact that the
371 artificial (linear) lin*Cdr1as*, when expressed in combination with knockdown of endogenous (circular)
372 *Cdr1as*, does not produce any additional reduction of miR-7 abundance. Under these conditions, an
373 unleashed Cyrano-driven TDMD activity acting on miR-7 might reach a limit in miR-7 degradation rate
374 which cannot be further enhanced by an additional TDMD-competent target such as lin*Cdr1as* (Figure
375 1). In contrast, in the presence of the *Cdr1as* circular RNA, the system would be set to intermediate

376 miR-7 degradation rates which could be further enhanced by other TDMD-competent RNAs such as
377 lin*Cdr1as* (see model in Appendix Figure S1). Notably, a similar protection phenomenon has been
378 observed in a prostate cancer cell line, where knockdown of circ*CSNK1G3* bearing TDMD-like binding
379 sites for miR-181b/d decreased the abundance of these microRNAs, while circ*CSNK1G3* overexpression
380 increased it (Chen *et al*, 2019) (Figure S2F).

381 The molecular basis explaining the functional differences between circRNAs and their cognate
382 linear transcripts in triggering TDMD might relate to structural properties affected by the circular-
383 linear topology. Previous work has shown that circRNAs possess a greater tendency to fold into more
384 stable short local secondary structures compared to their linear counterpart transcripts (Liu *et al*,
385 2019). This may affect the flexibility of the miRNA binding region, a key factor for TDMD activity
386 (Pawlica *et al*, 2016; Li *et al*, 2021b; Fuchs Wightman *et al*, 2018), either enhancing or limiting TDMD
387 efficacy in different sequence contexts. In line with this idea, binding of TDMD-competent target RNAs
388 appears to drive a conformational change on AGO proteins (loaded with specific miRNAs) that leads to
389 their poly-ubiquitination by the ubiquitin ligase ZSWIM8 and its subsequent degradation. This would
390 leave the specific miRNAs unprotected and susceptible to degradation by general nucleases (Shi *et al*,
391 2020; Han *et al*, 2020). The more stable folding of circRNAs could either preclude or enhance the
392 conformational change of AGO, thus bypassing or boosting TDMD, respectively. Such folding might
393 also limit the length-dependent effects of circRNA relative to linear RNA (Figure 4) by reducing their
394 range of possible adopted conformations. This would be in line with our results showing that circRNA
395 length had no influence on their impact on miRNA stability (Figure 4) or the degree of pairing to
396 miRNAs (Figure EV5C) and with a recent report suggesting that circRNAs might bind to miRNAs more
397 efficiently than their cognate linear RNAs (Petkovic *et al*, 2021). Alternatively, whether the effect of
398 topology leads to reduced or enhanced TDMD activity might relate to specific sequence elements that
399 are located outside of the miRNA site *per se* for efficient triggering of TDMD (Lee *et al*, 2013;
400 Kleaveland *et al*, 2018; Han *et al*, 2020; Li *et al*, 2021b). Such sequences might be absent, more exposed
401 or simply occluded within the more highly structured circRNAs, possibly explaining the differences in
402 TDMD relative to their linear counterparts.

403 The topology-dependent effects on TDMD could also relate to the presence of a 5'-cap and a poly-
404 A tail. However, the latter seems dispensable for TDMD based on the fact that HSUR-1, which lacks a

405 poly-A tail, effectively drives TDMD on miR-27 (Cazalla *et al*, 2010; Pawlica *et al*, 2016). Likewise, by
406 showing that circRNAs can induce TDMD, our data present the first evidence that the 5'-cap is also
407 dispensable for this activity and that TDMD is not an exclusive property of linear RNAs.

408 Interactions between miRNAs and competing endogenous RNAs (ceRNAs) have received broad
409 attention in recent years as they might represent a mechanism of miRNA inhibition (Tay *et al*, 2014).
410 However, due to stoichiometry considerations, the likelihood that individual ceRNAs titrate the total
411 amount of miRNA available for target repression seems limited (Denzler *et al*, 2014; Jens & Rajewsky,
412 2015; Bosson *et al*, 2014; Pinzón *et al*, 2017; Denzler *et al*, 2016). Instead, models where multiple
413 ceRNAs regulate single miRNAs have been favoured (Ameres & Zamore, 2013; Dodbele *et al*, 2021).
414 The case of *Cdr1as*-miR-7 pairing might represent an outstanding example that functions in an
415 analogous way. *Cdr1as* is a highly expressed circRNA in human, rat and mouse brain with > 60
416 evolutionarily conserved miR-7 binding sites (Memczak *et al*, 2013; Hansen *et al*, 2013), significantly
417 exceeding the average number of sites annotated for circRNAs (based on Starbase/ENCORI database,
418 see Dataset EV2). On the other hand, miR-7 tends to display medium to low expression, resulting in a
419 *Cdr1as*-miR-7 stoichiometry that is compatible with *Cdr1as* protection of this miRNA. Therefore, our
420 results favour a model where the concerted interaction of multiple circRNAs with individual miRNAs
421 seems the most likely and relevant scenario in regulating miRNA stability. Interestingly, among the
422 miRNAs that are upregulated upon ZSWIM8 knockdown in mouse induced neurons (Shi *et al*, 2020),
423 two belong to the most highly circRNA-paired miRNAs according to our analysis (miR-7 and also miR-
424 409-3p), suggesting that such type of regulation might be acting in neuron differentiation and
425 possibly in pathophysiological conditions (Figure EV5B).

426 An increasing number of TDMD natural examples have arisen in the past few years, including both
427 endogenous and viral transcripts (Ameres *et al*, 2010; Cazalla *et al*, 2010; Bitetti *et al*, 2018; Ghini *et al*,
428 2018; Li *et al*, 2021b; Simeone *et al*, 2022; Kingston *et al*, 2022). Furthermore, the discovery that TDMD
429 is more widespread than initially thought suggests that more examples will be discovered (Shi *et al*,
430 2020; Han *et al*, 2020). In this scenario, the apparent immunity of circRNAs to miRNA-mediated
431 degradation could confer them an advantage in regulating miRNA stability even (or especially) when
432 involving highly complementary TDMD-compatible architectures that would lead to target
433 degradation in the context of linear RNAs. Our findings support this view by suggesting that the most

434 highly paired miRNAs seem to engage in TDMD-like interactions with circRNAs more frequently than
435 the least paired miRNAs. Accordingly, by binding miRNAs through TDMD-like architectures, certain
436 combinations of circRNAs might either stabilize or degrade specific miRNAs even when expressed at
437 an overall sub-stoichiometric level relative to the whole set of linear targets present in the cell. This
438 type of regulation could in turn be compatible with a potential reversibility of a subset of circRNA's
439 inhibitory function on miRNAs.

440 A yet unresolved aspect of the role of circRNAs in regulating miRNAs relates to our inability to
441 predict their outcome on canonical miRNA silencing activity. Different outcomes may be expected
442 depending on the binding site architectures and the relative stoichiometries of the molecules
443 involved. For instance, miR-7 stabilization by *Cdr1as* in primary neurons and mouse cortex leads to
444 greater average target repression (Appendix Figure S2A-C), which is consistent with increased miRNA
445 abundance. In contrast, miR-181b/d stabilization by circ*CSNK1G3* leads to the opposite outcome: a
446 decreased overall target repression despite increased miRNA abundance (Appendix Figure S2D-E).
447 Based on this, a direct correlation between the eventual stabilization of miRNAs by circRNAs and their
448 ensuing downstream effect on miRNA canonical silencing cannot be currently established,
449 highlighting the need for further dissecting the role of circRNAs on miRNA target repression.
450 Eventually, more in-depth knowledge of the players involved, their relative stoichiometries and
451 dynamics will help us understand the emergent properties arising from different systems and the full
452 potential and adaptive value of circRNAs in miRNA regulation.

453

454 **Limitations of the study**

455 In this study, we have generated a set of vectors capable of expressing a circRNA with reduced
456 levels of linear "leak" RNA that is otherwise inevitably produced from these kinds of constructs. The
457 principle works in our hands, but the net circRNA-to-linear RNA relative expression yield that we
458 obtain is still suboptimal for the circRNA-expressing construct bearing ZKSCAN1 introns tested in
459 neurons. Bearing this limitation in mind, our data support the notion that the circRNA levels that we
460 achieve with this construct are enough to prevent TDMD, either by not contributing to any additional
461 TDMD effect and/or by antagonizing the TDMD driven by its co-expressed linear counterpart. The

462 opposite is true for the circRNA-expressing construct bearing *Lacasse2* introns tested in HEK293T cells.
463 We are aware that both technical and biological differences might account for the observed
464 differences.

465 It is important to stress that the diverse properties of different circRNAs might determine their
466 ability to affect TDMD, including but not limited to circRNA modifications (RNA methylation, etc) and
467 specific secondary structures, none of which have been systematically addressed in our work.
468 Likewise, more studies will be required to determine if the predominant effect of circRNAs is towards
469 blocking or enhancing TDMD.

470 Furthermore, we have shown that a group of miRNAs with high predicted pairing to circRNAs is
471 preferentially upregulated across neuron-like differentiation. It is worth emphasizing that this
472 correlation does not imply causality and that functional experiments will be needed in the future to
473 validate this possibility. Finally, the enrichment of TDMD-like sites that we report in this study is based
474 solely on predicted –though not experimentally validated– sites using the scanMiR bioinformatic tool
475 (Soutschek *et al*, 2022).

476

477 # Materials and methods

478 ## Plasmid construction

479 Unless otherwise specified, the lentiviral vectors are based on pRRLSIN.cPPT.SYN.WPRE (de la Mata
480 *et al*, 2015).

481 Linear *Cdr1as* (lin*Cdr1as*) was amplified by PCR from rat genomic DNA (see primers at Table EV1).
482 Following gel purification (QIAquick Gel Extraction Kit) and cloning into pCR II-Blunt-TOPO
483 (ThermoFisher), it was then subcloned into pRRLSIN.cPPT.SYN.WPRE. The linear *Cdr1as* version lacking
484 the sh*Cdr1as* target site –lin*Cdr1as*$^{671-}$ was generated by PCR amplification of a *Cdr1as* fragment
485 lacking a 174-bp 3'-terminal segment that encompasses the miR-671 binding site, and re-cloning it
486 into the original backbone's BamHI-SalI sites (Table EV1). The linear transcript used as a negative
487 control consists of GFP expressed from pRRLSIN.cPPT.PGK-GFP.WPRE (Addgene plasmid 12252).

488 The pri-miR-132 and pri-miR-124 expressing constructs were made by amplifying the pri-miRNA
489 fragments (Table EV1) from miRNASelectTM pEGP-mmu-mirna expression vectors (Cell Biolabs) and
490 subsequently cloning them into the BamHI-BsrGI sites of pRRLSIN.cPPT.SYN.WPRE.

491 The shRNAmiR (sh*Cdr1as*) is an engineered version miR-671 –previously described as a natural
492 *Cdr1as* regulator (Piwecka *et al*, 2017; Kleaveland *et al*, 2018)– designed to be fully complementary to
493 the circRNA and maximizing its slicing capacity (Figure EV1A). The sh*Cdr1as* lentiviral vector was
494 constructed by replacing the pri-miRNA fragments from the previously described vectors using
495 BamHI-NheI (Table EV1), and inserting a synthetic DNA (gBlock gene fragment, IDT) by Gibson
496 Assembly (Gibson *et al*, 2009).

497 CircRNA-expressing constructs were constructed inserting gBlocks (Integrated DNA Technologies)
498 encompassing the ZKSCAN1 upstream and downstream introns (Liang & Wilusz, 2014) flanking
499 mCherry and bulged or seed-mutant miR-132 sites (de la Mata *et al*, 2015) downstream of a
500 Tetracycline-inducible promoter (TREp, see Figure 2A and Table EV1). Perfect or seed-mutant sites for
501 miR-124 were subsequently inserted downstream or the circularizable region (Figure EV2A). Linear
502 TDMD inducers expressing mCherry upstream of bulged or seed-mutant miR-132 sites were
503 previously described (de la Mata *et al*, 2015). To replace the miR-124 sites by miR-92a sites, we
504 introduce a g-block with the relevant sequence into the BsrGI-SalI sites using Gibson Assembly
505 (Gibson *et al*, 2009) (for the g-block sequence see Table EV1).

506 Constructs expressing artificial circRNAs of different sizes are based on the pcDNA3.1(+) Laccase2
507 MCS Exon Vector (Addgene 69893). We inserted a perfectly matched or seed-mutant site for miR-92a
508 using the NotI and ApaI sites located between the Laccase2 intron and the poly(A) site (see oligos in
509 Table EV1). For the long circRNA, a BamHI-NotI fragment with split-GFP circRNA from the pcDNA3.1(+)
510 Laccase2 MCS-UNC circGFP (kindly provided by the Wilusz Lab) was inserted into the previous
511 constructs. Finally, an insert obtained by assembly PCR with miR-218 sites (TDMD-competent or seed-
512 mutant) was introduced into the BsrGI site located between the end of GFP and the IRES (see oligos in
513 Table EV1). The miR-218 site was based on the naturally occurring TDMD site in TRIM9, together with
514 the 20 nucleotides flanking it (Li *et al*, 2021a). The linear controls were generated by introducing the
515 corresponding PCR products into the NheI-XbaI sites of pcDNA3.1(+) (see oligos in Table EV1). To
516 generate the shorter circRNA and corresponding linear control, we amplified a shorter version of the

517 circRNA comprising half of GFP and a part of the IRES (see oligos in Table EV1) and inserted it into the
518 AgeI-SacII or NheI-XbaI sites of the circular and linear long constructs respectively. All constructs were
519 sequenced to verify splicing and miRNA binding sites integrity.

520 The lentiviral vector driving expression of FLAG/HA-AGO2 (human) from the Syn promoter (pLV-
521 FLAG-HA_AGO2) was generated by amplifying FLAG/HA-AGO2 from pIRESneo-FLAG/HA AGO2
522 (Addgene plasmid 10822).

523 The construct for CRISPR/Cas9 genome editing of *Cdr1as* splicing sites is based on lentiCRISPRv2
524 (Addgene plasmid 52961), following the Zhang Lab protocol (Sanjana *et al*, 2014; Shalem *et al*, 2014)
525 (Primers in Table EV1).

526

527 **HEK293T culture and transient transfection**

528 HEK293T cells were available in our institute. Cells were tested for mycoplasma contamination and
529 only clean stocks were further used for our experiments. Cells were grown in DMEM-F12 (Gibco)
530 supplemented with 10% (v/v) FCS and 25 U/mL Penicillin-Streptomycin (Gibco) and were plated for
531 transfection at 100,000 cells/well on 24-well plates. One day after plating, cells were transfected using
532 the PEI method as previously described (de la Mata *et al*, 2015).

533

534 **Lentivirus production and transduction**

535 Recombinant lentiviral particles were produced in HEK293T cell line. Cells were co-transfected
536 using the PEI method with the lentiviral expression vector and two 2nd generation lentiviral
537 packaging vectors: pMD2.G expressing the VSV-G envelope gene (Addgene plasmid 12259) and
538 pCMVR8.74 expressing the gag/pol genes (Addgene plasmid 22036). The supernatants containing the
539 viral particles were collected 48–72 h after transfection, concentrated using centrifugal filter units
540 (Amicon Ultra-15, molecular weight cutoff 100 kDa, Millipore Cat. #UFC910024) as further checked as
541 previously described (de la Mata *et al*, 2015).

542

543 **Animals used in this study**

544 All animal tissues used in this study were obtained under experiment protocol no. No.2020-04-DR
545 with the approval from the Comisión Institucional para el Cuidado y Uso de los Animales de
546 Laboratorio (CICUAL) at the Instituto de Investigación en Biomedicina de Buenos Aires (IBioBA) –
547 CONICET – Partner Institute of the Max Planck Society.
548

549 **Neuronal cultures and lentiviral transduction**

550 Cortical and hippocampal neurons were dissected from embryonic day 16.5 and 18.5 (E16.5 and
551 E18.5), respectively, CD1 embryos of mixed sex. Culture preparation was performed as previously
552 described (Giusti *et al*, 2014; Vogl *et al*, 2015). Briefly, cortex from CD1 mouse embryos were dissected
553 and a neuronal suspension was prepared through Trypsin digestion and mechanical disruption of the
554 tissue. Neurons were plated in 24 multi-well plates at a density of 80cells/mm2 (150.000 cells per well)
555 and maintained in Neurobasal-A media (ThermoFisher) with 2% B27 and 0.5 mMGlutaMAX-I
556 (ThermoFisher) at 37 °C and 5% CO2. CD1 mice for neuronal cultures were provided by our Specific
557 Pathogen Free Animal Facility.

558 The euthanasia of the animals to generate primary neuronal cultures was performed under
559 experiment protocol no. 2020-04-DR which was evaluated by the Institutional Animal Care and Use
560 Committee of the IBioBA-CONICET according to the Principles for Biomedical Research involving
561 animals of the Council for International Organizations for Medical Sciences and provisions stated in
562 the Guide for the Care and Use of Laboratory Animals.

563 Neurons were transduced 4-7 days after plating (DIV4-7) with lentiviral constructs: lin*Cdr1as*$^{671-}$,
564 sh*Cdr1as*, the linear control or a combination of these, appropriately described in Results and Figures.
565 The vectors driving each of the circRNA-expressing constructs were transduced in combination with a
566 lentiviral construct expressing the tetracycline-controlled transactivator protein (LV-Syn-tTA). RNA was
567 extracted at DIV11 as indicated below.
568

569 **FLAG/HA-AGO2 transfection and immunoprecipitation (AGO2 RIP)**

570 The FLAG/HA-AGO2 expressing plasmid was transfected into HEK293T cells as described above.
571 Immunoprecipitation of FLAG/HA-AGO2 was performed with Anti-FLAG M2 Magnetic Beads (Sigma
572 Cat # M8823). Beads were washed twice with TBS buffer (50 mM Tris HCl, 150 mM NaCl, pH 7.4). For

573 each immunoprecipitation (IP), one 6-cm plate with 50% confluency was used. Cells were washed
574 once with cold PBS and lyzed in 500 µl of lysis buffer [50 mM Tris–HCl pH 7.5, 150mM NaCl, 1% (v/v)
575 TRITON X-100, 1 mM EDTA, containing protease inhibitors (cOmplete, EDTA-free Protease Inhibitor
576 Cocktail, Roche) and RNase inhibitor (Invitrogen)]. The lysates were incubated 30 minutes on ice,
577 cleared by centrifugation at 16,000 g for 10 minutes at 4 degrees and mixed with the washed beads.
578 After 2 hours of rotation at 4 degrees, the beads were washed three times with TBS buffer. As a control
579 for the IPs, non-transfected HEK293T cells were used. FLAG/HA-AGO2 expression and
580 immunoprecipitation efficiency were determined by Western blot using anti-HA antibody (clone 3F10,
581 Roche). RNA was extracted by adding Trizol reagent (Invitrogen) directly on the beads.
582

583 **Subcellular fractionation**

584 Briefly, the circRNA-expressing construct and the linear control were transfected into HEK293T cells
585 as described above, in 6-well plates at 50% confluency. After 48 hours, cells were harvested using 500
586 µl of PBS, transferred to a microcentrifuge tube and centrifuged at 500 g for 5 minutes. The
587 supernatant was discarded, and the pellet resuspended in 350 µl of PBS plus 0.1% NP-40 (IGEPAL). 150
588 µl were separated and called TOTAL fraction. The remaining volume was centrifuged for 10 seconds
589 at 10,000 rpm. 150 µl of the supernatant were separated and called CYTOPLASM fraction. The pellet
590 was resuspended in 150 µl of PBS plus 0.1% NP-40 (IGEPAL) and centrifuged again at 10,000 rpm. The
591 supernatant was discarded, and the pellet resuspended in 150 µl of PBS plus 0.1% NP-40 (IGEPAL).
592 This was called the NUCLEAR fraction.
593 Out of the 150 µl of each fraction, 75 µl were used for Western Blotting and 75 µl for RNA
594 extraction followed by reverse transcription and quantitative polymerase chain reaction (RT-qPCR).
595

596 **RNA extraction**

597 Total RNA extractions were made using Trizol reagent (Invitrogen) following the manufacturer's
598 instructions.
599

600 **RT-qPCR quantification**

601 MiRNA and *U6* expression levels were determined by using Taqman® microRNA Assays (Applied
602 Biosystems) following the manufacturer's instructions or using SYBR Green and step-loop RT-qPCR
603 (see Table EV3 for oligo design). MicroRNA levels were normalized to *U6* RNA levels. Standard curves
604 for the analysed miRNAs and *U6* RNA were performed with serial dilutions of selected cDNAs, allowing
605 calculation of relative abundances. For quantification of target mRNAs, the artificial circRNA and
606 *Cdr1as*, total RNA was treated with RNase-free DNase I (DNA-freeTM Kit, Ambion) and reverse
607 transcribed using random hexamers and SuperScriptTM II Reverse Transcriptase (Invitrogen) or MMLV-
608 RT (Sigma), following the manufacturer's instructions. The abundance of target mRNAs, artificial
609 circRNA and *Cdr1as* were determined by SYBR green qPCR using a custom-made qPCR mix (Table EV2)
610 and specific primers (detailed at Table EV3). Alternatively, INBIO highway qPCR SYBR green mix was
611 used (Ref M130). Standard curves for the analysed amplicons were performed with serial dilutions of
612 selected cDNAs, allowing calculation of relative abundances.
613

614 **Northern blot analysis**

615 Northern blot analysis was performed according to standard procedures (Roditi *et al*, 1987). A total
616 of 10 μg RNA was loaded in each lane. The radioactively labelled probe, corresponding to the mCherry
617 CDS fragment, was prepared using the Megaprime DNA labelling kit (Amersham Biosciences)
618 according to manufacturer's instructions. Alternatively, biotin-labeled oligonucleotide probes were
619 used together with chemiluminescent nucleic acid detection kits according to manufacturer's
620 instructions (Thermo Scientific). The 18S RNA from the agarose gel run was used as loading control.
621 Blots were hybridized at 65° and washed in 0.2× SSC/0.1% SDS. The blots were exposed to
622 Phosphorimager screens and scanned with Typhoon FLA 7000 (GE Healthcare Life Sciences) or
623 exposed to X-ray film. The relative intensities of the bands were measured by densitometry using
624 ImageJ.
625

626 **Western blot analysis**

627 Protein samples were separated on 12% SDS-polyacrylamide gels and transferred to PVDF
628 membranes. Membranes were incubated with primary antibodies: anti-HA 3F10 (Rat, 1:2500), anti-
629 Tubulin (polyclonal rabbit anti β Tubulin H-235 from Santa Cruz Biotechnology, 1:2500) and Histone-3

630 (polyclonal rabbit anti H3 H-0164 from Merk, 1:2500). After washing, membranes were incubated with
631 IRDye® 800CW (LI- COR Biosciences) secondary antibodies. Bound antibody was detected an Odyssey
632 imaging system (LI-COR Biosciences).
633

634 **Statistical analysis**

635 R programming language was used to process information, visualize and design graphs, and
636 perform statistical tests. Data was normalized and scaled across experiments using Unit Length
637 Normalization. Bar, line, scatter, dot and boxplots were designed using the ggplot2 (Wickham, 2016)
638 and ggpubr packages. Statistical tests were done using base R and/or ggpubr (and its complement
639 rstatix) (https://rpkgs.datanovia.com/ggpubr/index.html). For experiments where two conditions
640 were compared, we performed unpaired t-tests, and for those where multiple comparisons were
641 made, we used the Bonferroni correction (ns: $p > 0.05$, *: $p <= 0.05$, **: $p <= 0.01$, ***: $p <= 0.001$, ****:
642 $p <= 0.0001$). For comparisons involving multiple groups we used either ANOVA followed by Tukey
643 multiple comparisons, Generalized Linear Models (GLM) with emmeans
644 (https://github.com/rvlenth/emmeans), or Wilcoxon rank sum test p-values (corrected with the
645 Hochberg method for multiple comparisons) as indicated in the text. When comparing several miR-7
646 targets across conditions, we performed a two-way ANOVA followed by Tukey multiple comparisons,
647 showing the adjusted p-value.
648

649 **Bioinformatic analysis of circRNA-miRNA interactions**

650 Two publicly available datasets produced by the Chen Lab were combined to generate a
651 comprehensive analysis taking into account miRNA, circRNA and mRNA expression during
652 differentiation of H9 (hESC) cells to H9 forebrain neurons. From GEO Accession GSE73325 (Zhang *et al*,
653 2016), we obtained data for circRNA and mRNA expression. From GEO Accessions GSE56152 and
654 GSE63709 (Chen *et al*, 2015), we obtained data for microRNA expression. Noteworthy, although the
655 same procedure for differentiation was followed (Zhang *et al*, 2016; Chen *et al*, 2015), sequencing was
656 done on different days (D26 and D35, respectively). We realize this is suboptimal, nevertheless we
657 proceeded with the analysis considering this the best data available to approach our questions.

658 Data of the interactions between circRNAs and miRNAs was retrieved from Starbase/ENCORI v3
659 database (http://starbase.sysu.edu.cn; (Yang *et al*, 2011; Li *et al*, 2014)). This particular source was
660 selected because it combines site prediction by several programs with experimental validation (e.g.,
661 by CLIP). The main parameters chosen for downloading through their API were: assembly = hg19,
662 geneType= circRNA & miRNA, clipExpNum=1, program= all, programNum= 2, target= all and
663 cellType= all.

664 A condensed spreadsheet summarizing all the previously mentioned data can be found at Dataset
665 EV3.

666 The analysis was done in R, briefly:

667 • The expression tables were loaded and merged using the Tidyverse package (Wickham *et al*,
668 2019) and/or the readxl package (Wickham & Bryan, 2022), while the circRNA-miRNA interactions
669 table was joined using the Fuzzyjoin package (https://CRAN.R-project.org/package=fuzzyjoin) to
670 consider genomic locations of both the circRNAs and the miRNA sites.

671 • Log_2 fold changes across differentiation were calculated for each type of RNA.

672

673 Analysis from a miRNA perspective:

674 • An absolute number of validated miRNA-specific sites on every circRNA (when present) was
675 calculated.

676 • A relative number of effective miRNA-specific sites was calculated by weighing the above
677 number (i.e. the absolute number of miRNA-specific sites on every circRNA) to the number of
678 backspliced junction reads as an estimate of the contribution of each circRNA.

679 • A total number of effective sites was calculated per miRNA (referred to as "miRNA-specific
680 effective sites" later on) by summing all the effective miRNA-specific sites among all circRNAs,.

681 • A miRNA-specific Pairing coefficient was defined by dividing the above number ("miRNA-specific
682 effective sites") by the miRNA abundance pre-differentiation. To simplify the analysis, we
683 separated miRNAs in quartiles of increasing pairing coefficients and performed the downstream
684 analysis based on them.

685

686 Analysis from a circRNA perspective:

687 • The sum of all (i.e. pooling all miRNAs) absolute numbers of validated miRNA sites on each
688 circRNA (when present) was calculated.
689 • The "pairing capacity" index for each circRNA was calculated by multiplying the above number to
690 the number of junction reads pre-differentiation.
691
692 All graphs were programmed and illustrated using the packages ggplot2 (Wickham, 2016), ggrepel
693 (https://CRAN.R-project.org/package=ggrepel) and/or viridis (https://CRAN.R-
694 project.org/package=viridis). The network diagram (Figure EV5A) was done using IGraph package
695 (https://igraph.org/r/). Statistical analysis of the boxplots was done and added to the graphs using
696 ggpubr (https://rpkgs.datanovia.com/ggpubr/index.html).
697 For pri-miRNA analysis we used the Galaxy platform (The Galaxy platform for accessible,
698 reproducible and collaborative biomedical analyses: 2022 update., 2022). Briefly, raw reads extracted
699 from GSE73325 were trimmed using Trim Galore! (https://github.com/FelixKrueger/TrimGalore) and
700 mapped to the human reference genome (hg38) with the RNA-STAR aligner (Dobin *et al*, 2013). Pri-
701 miR counts were obtained from the mapped BAM files using featureCounts (Liao *et al*, 2014) and the
702 annotation file (has.gff3) retrieved from miRBase (Kozomara *et al*, 2019).
703

704 **Bioinformatic prediction of TDMD-like sites on circRNAs**

705 To predict TDMD-like sites on circRNAs, we used the scanMiR package (Soutschek *et al*, 2022).
706 Briefly, all reported human circRNA sequences were retrieved from circBase (Glažar *et al*, 2014) and
707 used as an input for the *findSeedMatches* function from scanMiR to predict TDMD-like sites for every
708 miRNA present. The data was filtered to keep only those sites on circRNAs that had at least one
709 junction read in the neuron-like differentiation data (see above). Finally, we calculated the proportion
710 of miRNAs with predicted TDMD-like sites (computed as those with at least one TDMD-like site on
711 circRNAs/linear RNAs) within each of the quartiles of increasing pairing coefficients. Fisher's Exact
712 tests between each quartile and the least paired quartile ("- paired") were performed to assess
713 enrichment. The ggpie and rstatix packages were used to generate the pie charts and the ggpubr
714 package to do the violin plot and t-tests.

715

716 **Bioinformatic analysis of miR-7 and miR-181b/d targets**

717 Targets for miR-7 were retrieved from TargetScan 7.1 mouse (Agarwal *et al*, 2015) while the ones
718 for miR-181b/d from TargetScan 7.2 human (Agarwal *et al*, 2015). Raw RNA-seq counts were
719 downloaded for *Cdr1as* KO data (Piwecka *et al*, 2017) and circCSNK1G3 KD (Chen *et al*, 2019),
720 accessions GSE93130 and GSE113124, respectively. A differential expression analysis was performed
721 using the DESeq2 package (Love *et al*, 2014). Graphs were made using the results of the analysis and
722 the packages mentioned above.

723

724 # Data availability

725 Scripts and functions used to produce the results and plots shown in this paper can be found at:
726 https://github.com/mmataLab/ciR-miR-stability

727

728 # Acknowledgements

729 We thank Isabel Roditi for providing materials and discussing experiments, Helge Grosshans**,**
730 Alberto R. Kornblihtt, and Javier Cáceres for a critical reading of the manuscript, Pierre-Luc Germain for
731 a critical reading and general discussion of the manuscript, Valeria Buggiano for technical assistance
732 and Luciana Giono for creating figure illustrations. M.d.l.M. is funded by grants from Agencia Nacional
733 de Promocion Cientifica y Tecnológica (ANPCyT) of Argentina (PICT- 2016-0499**,** PICT-2018-0478_PRH
734 2016-0002 and PICT-2020-SERIEA-03100). D.R. acknowledges the support of the Volkswagen, Stiftung,
735 the Max Planck Society, the Fondo para la Convergencia Estructural de Mercosur (COF 03/11), the
736 Agencia Nacional de Promoción Científica y Tecnológica (ANPCyT) of Argentina (PICT- 2019-0499 and
737 PICT-PRH 2014-3782) and the Ministerio de Ciencia, Tecnología e Innovación Productiva of Argentina
738 (MinCyT-BMBF AL15/10). J.P.F. is funded by grants from Ministerio de Ciencia, Tecnología e Innovación
739 Productiva of Argentina (MINCyT) (BMBF/MINCYT MIGRAMIRNA AI/17/05), Agencia Nacional de
740 Promocion Cientifica y Tecnologica (ANPCyT) of Argentina (PICT-2017-2401, PCE-GSK-2017-0052),
741 Glaxo-SmithKline (PCE-GSK-2017-0052) and Fundación Progreso de la Medicina (GF N03/2017). J.E.W.
742 is supported by National Institutes of Health grant R35-GM119735 and Cancer Prevention & Research
743 Institute of Texas grant RR210031. J.E.W. is a CPRIT Scholar in Cancer Research. F.F.W. received a Ph.D.

fellowship from the National Scientific and Technical Research Council (CONICET) of Argentina and an IUBMB Wood-Whelan short-term research fellowship to visit the Wilusz lab.

Author contributions

F.F.W., D.R. and M.d.l.M. conceived the project and designed and interpreted the experiments. F.F.W. and J.L. designed, performed and interpreted most of the experiments. F.F.W. conceived, performed and interpreted most of the computational analysis. M.d.l.M. conceived, performed and interpreted some of the computational analysis. G.S. and M.S. contributed with the use of the scanMiR package to obtain the TDMD-like site enrichment results and discussed strategies for data analysis. J.L. and S.G. handled animals and prepared the neuron primary cultures. L.B. performed the subcellular fractionation experiments. F.F.W., B.P. and R.F. performed the Northern blot analysis. P.G. performed the subcloning of some of the constructs used in the study. J.P.F. designed some of the experiments and discussed experimental strategies. J.E.W., D.R. and M.d.l.M. supervised the whole project. The manuscript was written by F.F.W., D.R. and M.d.l.M.

Conflict of interest

J.E.W. serves as a consultant for Laronde.

761 # References

762 Agarwal V, Bell GW, Nam JW & Bartel DP (2015) Predicting effective microRNA target sites in
763 mammalian mRNAs. *eLife* 4: 1–38

764 Ameres SL, Horwich MD, Hung J-H, Xu J, Ghildiyal M, Weng Z & Zamore PD (2010) Target RNA-directed
765 trimming and tailing of small silencing RNAs. *Science* 328: 1534–1539

766 Ameres SL & Zamore PD (2013) Diversifying microRNA sequence and function. *Nat Rev Mol Cell Biol* 14:
767 475–488

768 Bartel DP (2018) Metazoan MicroRNAs. *Cell* 173: 20–51

769 Bitetti A, Mallory AC, Golini E, Carrieri C, Carreño Gutiérrez H, Perlas E, Pérez-Rico YA, Tocchini-Valentini
770 GP, Enright AJ, Norton WHJ, *et al* (2018) MicroRNA degradation by a conserved target RNA
771 regulates animal behavior. *Nat Struct Mol Biol* 25: 244–251

772 Bosson AD, Zamudio JR & Sharp PA (2014) Endogenous miRNA and target concentrations determine
773 susceptibility to potential ceRNA competition. *Mol Cell* 56: 347–359

774 Brown BD, Gentner B, Cantore A, Colleoni S, Amendola M, Zingale A, Baccarini A, Lazzari G, Galli C &
775 Naldini L (2007) Endogenous microRNA can be broadly exploited to regulate transgene
776 expression according to tissue, lineage and differentiation state. *Nat Biotechnol* 25: 1457–
777 1467

778 Cazalla D, Yario T & Steitz JA (2010) Down-regulation of a host microRNA by a Herpesvirus saimiri
779 noncoding RNA. *Science* 328: 1563–1566

780 Chen L-L (2020) The expanding regulatory mechanisms and cellular functions of circular RNAs. *Nat Rev*
781 *Mol Cell Biol* 21: 475–490

782 Chen S, Huang V, Xu X, Livingstone J, Soares F, Jeon J, Zeng Y, Hua JT, Petricca J, Guo H, *et al* (2019)
783 Widespread and Functional RNA Circularization in Localized Prostate Cancer. *Cell* 176: 831-
784 843.e22

785 Chen T, Xiang J-F, Zhu S, Chen S, Yin Q-F, Zhang X-O, Zhang J, Feng H, Dong R, Li X-J, *et al* (2015)
786 ADAR1 is required for differentiation and neural induction by regulating microRNA
787 processing in a catalytically independent manner. *Cell Res* 25: 459–476

788 Chu J, Robert F & Pelletier J (2021) Trans-spliced mRNA products produced from circRNA expression
789 vectors. *RNA* 27: 676–682

790 Conn SJ, Pillman KA, Toubia J, Conn VM, Salmanidis M, Phillips CA, Roslan S, Schreiber AW, Gregory PA
791 & Goodall GJ (2015) The RNA binding protein quaking regulates formation of circRNAs. *Cell*
792 160: 1125–1134

793 de la Mata M, Gaidatzis D, Vitanescu M, Stadler MB, Wentzel C, Scheiffele P, Filipowicz W & Großhans H
794 (2015) Potent degradation of neuronal miRNAs induced by highly complementary targets.
795 *EMBO Rep* 16: 500–511

796 Denzler R, Agarwal V, Stefano J, Bartel DP & Stoffel M (2014) Assessing the ceRNA hypothesis with
797 quantitative measurements of miRNA and target abundance. *Mol Cell* 54: 766–776

798 Denzler R, McGeary SE, Title AC, Agarwal V, Bartel DP & Stoffel M (2016) Impact of MicroRNA Levels,
799 Target-Site Complementarity, and Cooperativity on Competing Endogenous RNA-Regulated
800 Gene Expression. *Mol Cell* 64: 565–579

801 Dobin A, Davis CA, Schlesinger F, Drenkow J, Zaleski C, Jha S, Batut P, Chaisson M & Gingeras TR (2013)
802 STAR: ultrafast universal RNA-seq aligner. *Bioinformatics* 29: 15–21

803 Dodbele S, Mutlu N & Wilusz JE (2021) Best practices to ensure robust investigation of circular RNAs:
804 pitfalls and tips. *EMBO Rep* 22: e52072

805 Fellmann C, Hoffmann T, Sridhar V, Hopfgartner B, Muhar M, Roth M, Lai DY, Barbosa IAM, Kwon JS,
806 Guan Y, *et al* (2013) An optimized microRNA backbone for effective single-copy RNAi. *Cell Rep*
807 5: 1704–1713

808 Fuchs Wightman F, Giono LE, Fededa JP & de la Mata M (2018) Target RNAs Strike Back on MicroRNAs.
809 *Front Genet* 9: 435

810 Gasparini S, Licursi V, Presutti C & Mannironi C (2020) The Secret Garden of Neuronal circRNAs. *Cells* 9:
811 1815

812 Ghini F, Rubolino C, Climent M, Simeone I, Marzi MJ & Nicassio F (2018) Endogenous transcripts
813 control miRNA levels and activity in mammalian cells by target-directed miRNA degradation.
814 *Nat Commun* 9: 3119

815 Gibson DG, Young L, Chuang R-Y, Venter JC, Hutchison CA 3rd & Smith HO (2009) Enzymatic assembly
816 of DNA molecules up to several hundred kilobases. *Nat Methods* 6: 343–345

817 Giusti SA, Vogl AM, Brockmann MM, Vercelli CA, Rein ML, Trümbach D, Wurst W, Cazalla D, Stein V,
818 Deussing JM, *et al* (2014) MicroRNA-9 controls dendritic development by targeting REST. *Elife*
819 3: e02755

820 Glažar P, Papavasileiou P & Rajewsky N (2014) circBase: a database for circular RNAs. *RNA* 20: 1666–
821 1670

822 Grimson A, Farh KK-H, Johnston WK, Garrett-Engele P, Lim LP & Bartel DP (2007) MicroRNA Targeting
823 Specificity in Mammals: Determinants beyond Seed Pairing. *Mol Cell* 27: 91–105

824 Gu S, Jin L, Zhang F, Sarnow P & Kay MA (2009) Biological basis for restriction of microRNA targets to
825 the 3′ untranslated region in mammalian mRNAs. *Nat Struct Mol Biol* 16: 144–150

826 Guarnerio J, Zhang Y, Cheloni G, Panella R, Mae Katon J, Simpson M, Matsumoto A, Papa A, Loretelli C,
827 Petri A, *et al* (2019) Intragenic antagonistic roles of protein and circRNA in tumorigenesis. *Cell*
828 *Res* 29: 628–640

829 Guo JU, Agarwal V, Guo H & Bartel DP (2014) Expanded identification and characterization of
830 mammalian circular RNAs. *Genome Biol* 15: 409

831 Han J, LaVigne CA, Jones BT, Zhang H, Gillett F & Mendell JT (2020) A ubiquitin ligase mediates target-
832 directed microRNA decay independently of tailing and trimming. *Science* 370: eabc9546

833 Hanan M, Simchovitz A, Yayon N, Vaknine S, Cohen-Fultheim R, Karmon M, Madrer N, Rohrlich TM,
834 Maman M, Bennett ER, *et al* (2020) A Parkinson's disease CircRNAs Resource reveals a link
835 between circSLC8A1 and oxidative stress. *EMBO Mol Med* 12: e11942

836 Hansen TB, Jensen TI, Clausen BH, Bramsen JB, Finsen B, Damgaard CK & Kjems J (2013) Natural RNA
837 circles function as efficient microRNA sponges. *Nature* 495: 384–388

838 Hansen TB, Wiklund ED, Bramsen JB, Villadsen SB, Statham AL, Clark SJ & Kjems J (2011) miRNA-
839 dependent gene silencing involving Ago2-mediated cleavage of a circular antisense RNA.
840 *EMBO J* 30: 4414–4422

841 Ho-Xuan H, Glažar P, Latini C, Heizler K, Haase J, Hett R, Anders M, Weichmann F, Bruckmann A, Van
842 den Berg D, *et al* (2020) Comprehensive analysis of translation from overexpressed circular
843 RNAs reveals pervasive translation from linear transcripts. *Nucleic Acids Res* 48: 10368–10382

844 Jeck WR, Sorrentino JA, Wang K, Slevin MK, Burd CE, Liu J, Marzluff WF & Sharpless NE (2013) Circular
845 RNAs are abundant, conserved, and associated with ALU repeats. *RNA* 19: 141–157

846 Jens M & Rajewsky N (2015) Competition between target sites of regulators shapes post-
847 transcriptional gene regulation. *Nat Rev Genet* 16: 113–126

848 Jonas S & Izaurralde E (2015) Towards a molecular understanding of microRNA-mediated gene
849 silencing. *Nat Rev Genet* 16: 421–433

850 Kingston ER, Blodgett LW & Bartel DP (2022) Endogenous transcripts direct microRNA degradation in
851 Drosophila, and this targeted degradation is required for proper embryonic development.
852 *Mol Cell*: S1097-2765(22)00849–8

853 Kleaveland B, Shi CY, Stefano J & Bartel DP (2018) A Network of Noncoding Regulatory RNAs Acts in
854 the Mammalian Brain. *Cell* 174: 350-362.e17

855 Kozomara A, Birgaoanu M & Griffiths-Jones S (2019) miRBase: from microRNA sequences to function.
856 *Nucleic Acids Res* 47: D155–D162

857 Kramer MC, Liang D, Tatomer DC, Gold B, March ZM, Cherry S & Wilusz JE (2015) Combinatorial control
858 of Drosophila circular RNA expression by intronic repeats, hnRNPs, and SR proteins. *Genes Dev*
859 29: 2168–2182

860 Kristensen LS, Andersen MS, Stagsted LVW, Ebbesen KK, Hansen TB & Kjems J (2019) The biogenesis,
861 biology and characterization of circular RNAs. *Nat Rev Genet* 20: 675–691

862 Krol J, Busskamp V, Markiewicz I, Stadler MB, Ribi S, Richter J, Duebel J, Bicker S, Fehling HJJ, Schubeler
863 D, *et al* (2010) Characterizing light-regulated retinal microRNAs reveals rapid turnover as a
864 common property of neuronal microRNAs. *Cell* 141: 618–631

865 Lee S, Song J, Kim S, Kim J, Hong Y, Kim Y, Kim D, Baek D & Ahn K (2013) Selective degradation of host
866 MicroRNAs by an intergenic HCMV noncoding RNA accelerates virus production. *Cell Host*
867 *Microbe* 13: 678–690

868 Li J-H, Liu S, Zhou H, Qu L-H & Yang J-H (2014) starBase v2.0: decoding miRNA-ceRNA, miRNA-ncRNA
869 and protein-RNA interaction networks from large-scale CLIP-Seq data. *Nucleic Acids Res* 42:
870 D92-97

871 Li L, Sheng P, Li T, Fields CJ, Hiers NM, Wang Y, Li J, Guardia CM, Licht JD & Xie M (2021a) Widespread
872 microRNA degradation elements in target mRNAs can assist the encoded proteins. *Genes &*
873 *development*: 1595–1609

874 Li L, Sheng P, Li T, Fields CJ, Hiers NM, Wang Y, Li J, Guardia CM, Licht JD & Xie M (2021b) Widespread
875 microRNA degradation elements in target mRNAs can assist the encoded proteins. *Genes Dev*
876 35: 1595–1609

877 Li X, Liu C-X, Xue W, Zhang Y, Jiang S, Yin Q-F, Wei J, Yao R-W, Yang L & Chen L-L (2017) Coordinated
878 circRNA Biogenesis and Function with NF90/NF110 in Viral Infection. *Mol Cell* 67: 214-227.e7

879 Liang D & Wilusz JE (2014) Short intronic repeat sequences facilitate circular RNA production. *Genes*
880 *and Development* 28: 2233–2247

881 Liao Y, Smyth GK & Shi W (2014) featureCounts: an efficient general purpose program for assigning
882 sequence reads to genomic features. *Bioinformatics* 30: 923–930

883 Liu CX, Li X, Nan F, Jiang S, Gao X, Guo SK, Xue W, Cui Y, Dong K, Ding H, *et al* (2019) Structure and
884 Degradation of Circular RNAs Regulate PKR Activation in Innate Immunity. *Cell* 177: 865-
885 880.e21

886 Love MI, Huber W & Anders S (2014) Moderated estimation of fold change and dispersion for RNA-seq
887 data with DESeq2. *Genome Biol* 15: 550

888 Marcinowski L, Tanguy M, Krmpotic A, Rädle B, Lisnić VJ, Tuddenham L, Chane-Woon-Ming B, Ruzsics
889 Z, Erhard F, Benkartek C, *et al* (2012) Degradation of cellular mir-27 by a novel, highly
890 abundant viral transcript is important for efficient virus replication in vivo. *PLoS Pathog* 8:
891 e1002510

892 Memczak S, Jens M, Elefsinioti A, Torti F, Krueger J, Rybak A, Maier L, Mackowiak SD, Gregersen LH,
893 Munschauer M, *et al* (2013) Circular RNAs are a large class of animal RNAs with regulatory
894 potency. *Nature* 495: 333–338

895 Pamudurti NR, Bartok O, Jens M, Ashwal-Fluss R, Stottmeister C, Ruhe L, Hanan M, Wyler E, Perez-
896 Hernandez D, Ramberger E, *et al* (2017) Translation of CircRNAs. *Mol Cell* 66: 9-21.e7

897 Pawlica P, Moss WN & Steitz JA (2016) Host miRNA degradation by Herpesvirus saimiri small nuclear
898 RNA requires an unstructured interacting region. *RNA* 22: 1181–1189

899 Petkovic S, Graff S, Feller N, Berghaus J, Ruppert V-P, Dülfer J & Sczakiel G (2021) Circular versus linear
900 RNA topology: different modes of RNA-RNA interactions in vitro and in human cells. *RNA Biol*
901 18: 674–683

902 Pinzón N, Li B, Martinez L, Sergeeva A, Presumey J, Apparailly F & Seitz H (2017) microRNA target
903 prediction programs predict many false positives. *Genome Res* 27: 234–245

904 Piwecka M, Glažar P, Hernandez-Miranda LR, Memczak S, Wolf SA, Rybak-Wolf A, Filipchyk A,
905 Klironomos F, Cerda Jara CA, Fenske P, *et al* (2017) Loss of a mammalian circular RNA locus
906 causes miRNA deregulation and affects brain function. *Science* 357: eaam8526

907 Roditi I, Carrington M & Turner M (1987) Expression of a polypeptide containing a dipeptide repeat is
908 confined to the insect stage of Trypanosoma brucei. *Nature* 325: 272–274

909 Rybak-Wolf A, Stottmeister C, Glažar P, Jens M, Pino N, Giusti S, Hanan M, Behm M, Bartok O, Ashwal-
910 Fluss R, *et al* (2015) Circular RNAs in the Mammalian Brain Are Highly Abundant, Conserved,
911 and Dynamically Expressed. *Mol Cell* 58: 870–885

912 Salzman J, Chen RE, Olsen MN, Wang PL & Brown PO (2013) Cell-type specific features of circular RNA
913 expression. *PLoS genetics* 9: e1003777

914 Sanjana NE, Shalem O & Zhang F (2014) Improved vectors and genome-wide libraries for CRISPR
915 screening. *Nat Methods* 11: 783–784

916 Shalem O, Sanjana NE, Hartenian E, Shi X, Scott DA, Mikkelson T, Heckl D, Ebert BL, Root DE, Doench
917 JG, *et al* (2014) Genome-scale CRISPR-Cas9 knockout screening in human cells. *Science* 343:
918 84–87

919 Shi CY, Kingston ER, Kleaveland B, Lin DH, Stubna MW & Bartel DP (2020) The ZSWIM8 ubiquitin ligase
920 mediates target-directed microRNA degradation. *Science* 370: eabc9359

921 Simeone I, Rubolino C, Noviello TMR, Farinello D, Cerulo L, Marzi MJ & Nicassio F (2022) Prediction and
922 pan-cancer analysis of mammalian transcripts involved in target directed miRNA degradation.
923 *Nucleic Acids Res* 50: 2019–2035

924 Soutschek M, Gross F, Schratt G & Germain P-L (2022) scanMiR: a biochemically-based toolkit for
925 versatile and efficient microRNA target prediction. *Bioinformatics*: btac110

926 Tay Y, Rinn J & Pandolfi PP (2014) The multilayered complexity of ceRNA crosstalk and competition.
927 *Nature* 505: 344–352

928 The Galaxy platform for accessible, reproducible and collaborative biomedical analyses: 2022 update.
929 (2022) *Nucleic Acids Res* 50: W345-351

930 Vogl AM, Brockmann MM, Giusti SA, Maccarrone G, Vercelli CA, Bauder CA, Richter JS, Roselli F, Hafner
931 A-S, Dedic N, *et al* (2015) Neddylation inhibition impairs spine development, destabilizes
932 synapses and deteriorates cognition. *Nat Neurosci* 18: 239–251

933 Wickham H (2016) Data Analysis. In *ggplot2: Elegant Graphics for Data Analysis*, Wickham H (ed) pp
934 189–201. Cham: Springer International Publishing

935 Wickham H, Averick M, Bryan J, Chang W, McGowan LD, François R, Grolemund G, Hayes A, Henry L,
936 Hester J, *et al* (2019) Welcome to the Tidyverse. *Journal of Open Source Software* 4: 1686

937 Wickham H & Bryan J (2022) readxl: Read Excel Files. *https://readxl.tidyverse.org,*
938 *https://github.com/tidyverse/readxl*

939 Xiao M-S, Ai Y & Wilusz JE (2020) Biogenesis and Functions of Circular RNAs Come into Focus. *Trends*
940 *Cell Biol* 30: 226–240

941 Yang J-H, Li J-H, Shao P, Zhou H, Chen Y-Q & Qu L-H (2011) starBase: a database for exploring
942 microRNA-mRNA interaction maps from Argonaute CLIP-Seq and Degradome-Seq data.
943 *Nucleic Acids Res* 39: D202-209

944 Yang L, Wilusz JE & Chen L-L (2022) Biogenesis and Regulatory Roles of Circular RNAs. *Annu Rev Cell*
945 *Dev Biol* 38: 263–289

946 You X, Vlatkovic I, Babic A, Will T, Epstein I, Tushev G, Akbalik G, Wang M, Glock C, Quedenau C, *et al*
947 (2015) Neural circular RNAs are derived from synaptic genes and regulated by development
948 and plasticity. *Nat Neurosci* 18: 603–610

949 Zhang XO, Wang HB, Zhang Y, Lu X, Chen LL & Yang L (2014) Complementary sequence-mediated
950 exon circularization. *Cell* 159: 134–147

951 Zhang Y, Xue W, Li X, Zhang J, Chen S, Zhang J-L, Yang L & Chen L-L (2016) The Biogenesis of Nascent
952 Circular RNAs. *Cell Rep* 15: 611–624

953

954 # Figure legends

955 **Figure 1.**

956 **The topology of *Cdr1as* determines the outcome of its effect on miR-7's stability.**

957 A *Cdr1as* total output levels (linear plus circular) measured by RT-qPCR upon transduction of either
958 a scrambled shRNA or sh*Cdr1as* alone, or sh*Cdr1as* rescued with a linear version of *Cdr1as*
959 (lin*Cdr1as*) lacking the *shCdr1as* site, in cortical primary neurons. n = 6 culture wells (from 3
960 independent primary cultures) for control and cirCDR1as KD; n = 4 culture wells (from 2
961 independent primary cultures) for lin*Cdr1as* rescue.

962 B MiR-7 abundance measured by Taqman RT-qPCR in the same samples as in A. n = 6 culture wells
963 (from 3 independent primary cultures) for control and cirCDR1as KD; n = 4 culture wells (from 2
964 independent primary cultures) for lin*Cdr1as* rescue.

965 C *Cdr1as* total output levels measured by RT-qPCR upon over-expression of linear *Cdr1as*
966 (lin*Cdr1as*) in primary hippocampal neurons. Control corresponds to a non-related (GFP-
967 expressing) linear transcript. n = 6 culture wells (from 2 independent primary cultures) for each
968 condition.

969 D MiR-7 abundance measured by Taqman RT-qPCR in the same samples as in C. n = 6 culture wells
970 (from 2 independent primary cultures) for each condition.

971 Data are presented as mean ± SEM. Statistical significance was determined by unpaired Student's *t*
972 *tests* (ns: $p > 0.05$, *: $p <= 0.05$, **: $p <= 0.01$, ***: $p <= 0.001$, ****: $p <= 0.0001$).

973

974 **Figure 2.**

975 **System to artificially express circRNAs reducing their overlapping, cognate linear RNA**
976 **expression.**

977 A. Top: Illustration of the linear RNA expressing construct used as a positive control for TDMD
978 (TDMD inducer). Bottom: Illustration of the circRNA-expressing construct; depicted with coloured
979 arrows are the sets of primers used to measure the different transcript variants (circular [1], Total
980 Output-TO [2] and linear [3]).

981 B. RT-qPCR measuring Total output (TO, primer pair #2), linear (primer pair #3) and circular
982 (divergent primer pair #1) RNA levels upon expression of the circRNA-expressing constructs from
983 the tetracycline-inducible promoter (TREp) bearing perfectly matched or seed-mutant miR-124
984 sites for selective linear RNA degradation (see Figure EV2A). Primers are depicted in Figure 2A. n
985 = 5 culture wells (from 3 independent primary cultures) of cortical neurons for each condition;
986 and n = 7 culture wells (from 4 independent primary cultures) of hippocampal neurons for each
987 condition.
988 C. Total reporter output (left) and circRNA levels (right) upon expression of the circRNA-expressing
989 construct or the linear RNA construct (TDMD inducer). The constructs were expressed from the
990 tetracycline-inducible promoter (TREp) and the synapsin (Syn) promoter respectively in order to
991 achieve similar total output levels for both constructs n = 9 culture wells (from 3 independent
992 primary cultures) of cortical neurons for each condition; n = 9 culture wells (from 4 independent
993 primary cultures) of hippocampal neurons for each condition. Missing points are failed culture
994 wells/RT-qPCR reactions.
995 In (B–C), data are presented as mean ± SEM. Statistical significance was determined by unpaired
996 Student's *t* tests (ns: p > 0.05, *: p <= 0.05, **: p <= 0.01, ***: p <= 0.001, ****: p <= 0.0001).
997
998 **Figure 3.**
999 **Artificial circRNA-expressing constructs are unable to trigger TDMD in primary neurons.**
1000 A RT-qPCR Taqman assay showing miR-132 abundance upon transduction of the linear control
1001 (left) or the circRNA-expressing construct (right) carrying bulged (TDMD-compatible) or seed-
1002 mutant miR-132 sites. n = 9 culture wells (from 3 independent primary cultures) of cortical
1003 neurons for each condition; n = 9 culture wells (from 4 independent primary cultures) of
1004 hippocampal neurons for each condition. Missing points are failed culture wells/RT-qPCR
1005 reactions.
1006 B AGO2-Flag immunoprecipitation (RIP) followed by RT-qPCR in HEK293T cells. MiR-27a was used
1007 to normalize expression. Relative circRNA abundance was measured using circRNA-backspliced-
1008 junction specific divergent primers and normalized to miR-27a levels as an unrelated RISC-loaded
1009 miRNA not expected to be affected by the circRNA. Levels of non-specific *U6* background

1010 binding to Ago2 are shown. As an IP quality control, FLAG/HA-AGO2 input levels were shown to
1011 be similar across transfected conditions and efficiently pulled-down using anti-FLAG beads
1012 (Figure EV3B). Accordingly, miR-27, but not *U6* RNA, was efficiently co-immunoprecipitated,
1013 showing an even recovery of Ago-bound RNA across transfected conditions (Figure EV3C). n = 4
1014 culture wells (from 2 experiments) of HEK293T cells for each condition.

1015 C Subcellular fractionation showing total vs. cytoplasmic (left) and total vs. nuclear (right) fractions,
1016 followed by RT-qPCR of the circRNA and linear RNA isoforms, normalized by *GAPDH* (for
1017 cytoplasm) or *U6* (for nucleus). Fractionation efficiency was assessed via Western Blot and RT-
1018 qPCR (Figure EV3D-E). n = 4 culture wells (from 2 experiments) of HEK293T cells for each
1019 condition.

1020 In (A–C), data are presented as mean ± SEM . Statistical significance was determined by unpaired
1021 Student's *t tests* (ns: p > 0.05, *: p <= 0.05, **: p <= 0.01, ***: p <= 0.001, ****: p <= 0.0001).

1022

1023

1024 **Figure 4.**

1025 **Artificial circRNA-expressing constructs trigger TDMD in HEK293T cells.**

1026 A Illustration of the constructs expressing linear or circular RNA of different sizes from a backbone
1027 containing *Drosophila laccase2* introns (Kramer *et al*, 2015).

1028 B Left: Northern blot analysis of samples from HEK293T cells expressing the constructs of the
1029 indicated length. n = 6 culture wells (from 2 independent experiments) of HEK293T cells for each
1030 condition. Right: Quantification by different methods of the linear and circular isoforms from
1031 samples of HEK293T cells expressing the indicated constructs. In red, the mean is indicated. NT
1032 are non-transfected cells.

1033 C MiR-218-5p abundance upon transduction of the linear controls (left) or the circRNA-expressing
1034 constructs (right) carrying bulged (TDMD-compatible) or seed-mutant miR-218-5 sites. n = 6
1035 culture wells (from 2 independent experiments) of HEK293T cells for each condition.

1036 Data are presented as mean ± SEM. Statistical significance was determined by unpaired Student's *t*
1037 *tests* (ns: p > 0.05, *: p <= 0.05, **: p <= 0.01, ***: p <= 0.001, ****: p <= 0.0001).

1038

1039 **Figure 5.**

1040 **CircRNAs potentially stabilize dozens of microRNAs across neuron-like differentiation.**

1041 A Scatter plot of miRNA expression fold changes (log2) across differentiation of hESC H9 cells into
1042 forebrain (FB) neuron progenitor cells plotted against the number of effective sites, coloured by
1043 quartiles of increasing number of "effective" sites within circRNAs.

1044 B Scatter plot of miRNA fold changes (log2) across differentiation plotted against miRNA-specific
1045 Pairing coefficient (log10) coloured by quartiles in a scatter plot. The predicted most highly
1046 paired miRNAs show the highest fold changes across differentiation.

1047 C Boxplot depicting the fold changes (log2) across differentiation of miRNA separated by quartiles
1048 of increasing miRNA-specific Pairing coefficients.

1049 D Scatter plots of miRNA fold changes (log2) plotted against pri-miRNA fold changes (log2) faceted
1050 by miRNA-specific Pairing coefficient quartiles. Indicated are the slopes (b) and p-values for the
1051 interaction terms of each quartile's curve against the reference ("- paired") quartile within a
1052 multiple regression model with interaction.

1053 E Boxplot showing circRNA expression fold changes (log2) across differentiation separated by
1054 quartiles of increasing "pairing capacity" index.

1055 The analysis includes 236 miRNAs. For panels C and E, GLM with emmeans statistics are shown
1056 between the least paired and the remaining groups (ns: $p > 0.05$, *: $p <= 0.05$, **: $p <= 0.01$, ***: $p <=$
1057 0.001, ****: $p <= 0.0001$).

1058

1059 **Figure 6.**

1060 **Predicted TDMD-like site architectures within circRNAs are more frequent for the most highly**
1061 **paired miRNAs.**

1062 A Pie charts showing the proportion of linear RNA- and circRNA-miRNA interactions involving at
1063 least one predicted TDMD-like site against miRNAs within quartiles of increasing miRNA-specific
1064 Pairing coefficient. Shown are the p-values for the Fisher's Exact test between each quartile and
1065 the least paired quartile ("- paired").

1066 B Violin plots depicting the number of predicted TDMD-like sites within circRNAs against miRNAs
1067 belonging to quartiles of increasing miRNA-specific Pairing coefficient. GLM with emmeans

statistics are shown between the least paired and the other quartiles (ns: p > 0.05, *: p <= 0.05, **: p <= 0.01, ***: p <= 0.001, ****: p <= 0.0001).

Expanded View Figure Legends

Figure EV1.

MicroRNA site illustrations, quality controls and primer design for *Cdr1as*.

A Scheme depicting the sequences of the miR-671 binding site within *Cdr1as*, miR-671 and the engineered sh*Cdr1as*. The latter is based on miR-671 with two nucleotide changes that make it fully complementary to the circRNA to maximize its slicing capacity.

B Illustration of the primer designs for measuring the different *Cdr1as* isoforms (detailed in Materials and Methods).

C Expression levels of *Cdr1as* total output, circular *Cdr1as* and unrelated gene (*Actb*) upon over-expression of linear *Cdr1as* (lin*Cdr1as*). Levels were normalized to *Gapdh*. n = 6 culture wells (from 2 independent primary cultures) for each condition.

D Expression levels of miR-7 guide strand (miR-7-5p), passenger strands (miR-7a-1-3p and miR-7a-2-3p), primary RNA (pri-miR-7a-1) and two unrelated miRNAs (miR-9-5p and miR-132-3p). All miRNAs levels were normalized to *U6*, while the pri-miR level was normalized to *Gapdh*. n = 6 culture wells (from 2 independent primary cultures) for each condition.

E Three examples of potential TDMD-competent binding sites for miR-7 present in *Cdr1as*, aligned and illustrated using scanMiR.

F Illustration of the strategy designed to mutate *Cdr1as* splicing sites by CRISPR/Cas9.

G *Cdr1as* total output levels upon CRISPR/Cas9 editing of the *Cdr1as* splicing sites, measured by RT-qPCR in primary hippocampal neurons. Control corresponds to a transduced linear transcript (GFP-expressing). n = 3 culture wells (from 1 independent primary culture) for each condition.

H MiR-7 abundance measured by Taqman RT-qPCR in the same samples as in F. n = 3 culture wells (from 1 independent primary culture) for each condition.

Data are presented as mean ± SEM. Statistical significance was determined by unpaired Student's *t tests* (ns: p > 0.05, *: p <= 0.05, **: p <= 0.01, ***: p <= 0.001, ****: p <= 0.0001). In panels C and D,

1096 Bonferroni's correction for multiple testing was applied. For the F and G panels, equal variance was
1097 assumed.
1098
1099 **Figure EV2.**
1100 **CircRNA-expressing constructs and quality controls.**
1101 A Table summarizing the generated constructs.
1102 B Northern blot analysis of RNase R treated or untreated samples from HEK293T cells expressing
1103 the indicated constructs with either perfect or seed-mutant miR-124 binding sites. CircRNAs are
1104 resistant to RNase R digestion, confirming the circular topology of the artificial circRNA. All
1105 constructs were expressed from the tetracycline-inducible promoter (TREp). The asterisk (*)
1106 marks a putative mechanically linearized product of the corresponding circRNA. Linear/circRNA
1107 ratio quantification was performed by digital densitometry using ImageJ.
1108 C Quantification by different methods of the linear and circular isoforms from RNase R untreated
1109 samples of HEK293T cells (naturally lacking miR124) expressing the indicated constructs. Top
1110 panels: digital densitometry quantification of Northern blot bands by ImageJ. Bottom panels: RT-
1111 qPCR quantification using primers specific for the circular isoform or for both the linear and
1112 circular isoforms combined (Total output) as depicted in Figure 2A. In red, the mean is indicated.
1113 n = 2 culture wells (from 1 experiment) of HEK293T cells for each condition.
1114 D RT-qPCR measurement of the circRNA-to-linear RNA ratio of RNase R treated vs. untreated
1115 samples in cortical neurons or HEK293T cells using divergent primers depicted in Figure 2. Values
1116 reflect relative rather than absolute ratios of the measured isoforms. n = 3 culture wells (from 1
1117 primary culture/experiment) of each cell type and for each condition.
1118 E Top: Agarose gel showing triplicates of the RT-qPCR amplicons obtained with divergent primers
1119 against the backsplicing junction of the artificial circRNA, after retro-transcription with two
1120 different reverse transcriptases (MMLV-RT & Superscript II) in order to rule out artifacts due to
1121 template switching during cDNA synthesis. Bottom: Sanger sequencing of the amplicons shown
1122 above confirming backsplicing junction in HEK293 cells.

1123 F Left: Northern blot analysis of in HEK293T cells expressing the indicated constructs bearing either
1124 perfect or seed-mutant miR-92a binding sites. Right: digital densitometry quantification of
1125 Northern blot bands by ImageJ.
1126 In (F), data are presented as mean ± SEM. Statistical significance was determined by unpaired
1127 Student's *t tests* (ns: p > 0.05, *: p <= 0.05, **: p <= 0.01, ***: p <= 0.001, ****: p <= 0.0001).
1128
1129 **Figure EV3.**
1130 **TDMD specificity, HA-FLAG/AGO2 RIP and cellular fractionation quality controls.**
1131 A RT-qPCR quantification of the indicated RNA species confirms specific degradation of miR-132
1132 guide strand (miR-132-3p) and discards potential transcriptional effects. Levels of miR-132
1133 passenger strand (miR-132-5p), primary transcript (pri-miR-132) and four unrelated miRNAs (miR-
1134 124-3p, miR-128-3p, miR-138-5p and miR-409-3p) were normalized to *U6*. n = 9 culture wells
1135 (from 3 independent primary cultures) of cortical neurons for each condition; n = 9 culture wells
1136 (from 4 independent primary cultures) of hippocampal neurons for each condition. Missing
1137 points are failed culture wells/RT-qPCR reactions.
1138 B Representative anti-HA Western Blot from inputs or anti-FLAG IPs in non-transfected HEK-293T
1139 cells or cells co-transfected with HA-FLAG/AGO2 and the circRNA-expressing construct bearing
1140 bulged (WT) or seed-mutant (mut) miR-132 sites.
1141 C *U6* and miR-27 levels were measured to verify the efficiency of HA-FLAG/AGO2
1142 immunoprecipitation. n = 4 culture wells (from 2 experiments) of HEK293T cells for each
1143 condition.
1144 D Representative Western Blot of HEK293T cells transfected with either the circRNA-expressing
1145 construct or the linear control RNA, following subcellular fractionation. β-Tubulin and Histone-3
1146 were used as cytoplasm and nucleus markers, respectively.
1147 E Boxplot depicting median values of *GAPDH*/*U6* ratio measured by RT-qPCR confirms proper
1148 subcellular fractionation of samples either transfected with the circRNA-expressing construct or
1149 the linear control. n = 4 culture wells (from 1 experiment) of HEK293T cells for each condition.

1150 In (A, C), data are presented as mean ± SEM. Statistical significance was determined by unpaired
1151 Student's *t tests* (ns: p > 0.05, *: p <= 0.05, **: p <= 0.01, ***: p <= 0.001, ****: p <= 0.0001). In
1152 panel A, Bonferroni's correction for multiple testing was applied.
1153
1154 **Figure EV4.**
1155 **CircRNA-expressing constructs and quality controls.**
1156 A Northern blot analysis of RNase R treated or untreated samples from HEK293T cells expressing
1157 the constructs of the indicated length. CircRNAs are resistant to RNase R digestion, confirming
1158 the circular topology of the artificial circRNA.
1159 B RT-qPCR quantification of the indicated RNA species confirms specific degradation of miR-218
1160 guide strand (miR-218-5p) and discards potential transcriptional effects. Levels of primary
1161 transcript (pri-miR-218) and one unrelated miRNA (miR-9-5p) were normalized to *U6*. n = 6
1162 culture wells (from 2 independent experiments) of HEK293T cells for each condition.
1163 Data are presented as mean ± SEM. Statistical significance was determined by unpaired Student's *t*
1164 *tests* (ns: p > 0.05, *: p <= 0.05, **: p <= 0.01, ***: p <= 0.001, ****: p <= 0.0001).
1165
1166 **Figure EV5.**
1167 **Illustrations of the predicted circRNA-miRNA networks and genomic features of the potentially**
1168 **involved circRNAs.**
1169 A Network diagram of biochemically supported interactions between circRNAs and miRNAs.
1170 Depicted are the interactions involving the seven most "pairing" circRNAs.
1171 B Network diagram showing biochemically supported circRNA-miRNA interactions for miR-7 and
1172 two other miRNAs with similar "pairing" coefficient (miR-670-3p and miR-409-3p). For all three
1173 examples, the stoichiometries (i.e. ratios of circRNA-binding-site:miRNA) are similar, with CDR1as
1174 making the largest contribution for miRNA-7. MiR-7 and miR-409 are also a demonstrated case
1175 and strong candidate to undergo of TDMD, respectively (see main text).
1176 C Boxplot showing the size of circRNAs (log2 of the base pairs) that interact with miRNAs from each
1177 of the different pairing quartiles estimated from data of hESC H9 into forebrain (FB) neuron

1178 progenitor cell differentiation (Chen *et al*, 2015; Zhang *et al*, 2016). Shown are Wilcoxon rank sum
1179 test p-values (corrected with the Hochberg method for multiple comparisons) between the least
1180 paired and the remaining groups (ns: $p > 0.05$).

1181 D Barplot representing the percentages of overlapping genomic regions (CDS, 5'UTR, 3'UTR, etc)
1182 giving rise to the circRNAs with predicted binding sites against miRNAs within different quartiles
1183 of miRNA-specific Pairing coefficient. No enrichment of genomics features for circRNAs
1184 interacting with miRNAs within the different quartiles was observed (Pearson's Chi-squared test
1185 p-value = 0.998).

1186

1187 **Figure EV6.**

1188 **Examples of predicted TDMD-like sites on circRNAs.**

1189 A Examples of TDMD-like sites within circRNAs predicted and aligned using scanMiR. The five
1190 miRNAs belong to the "+++ paired" quartile.

1191 B-C Pie charts showing the proportion of and circRNA-miRNA (B) and linear RNA-miRNA (C)
1192 interactions involving at least one predicted TDMD-like site against miRNAs within quartiles of
1193 increasing miRNA-specific Pairing coefficient. Shown are the p-values for the Fisher's Exact test
1194 between each quartile and the least paired quartile ("- paired").

1195

Figure 1

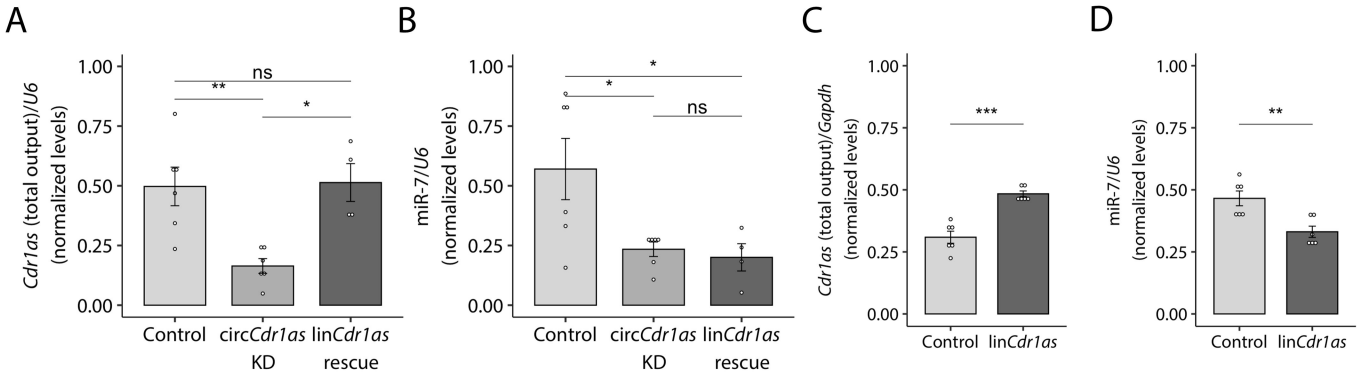
A
B
C
D
Cdr1as (total output)/U6 (normalized levels)
miR-7/U6 (normalized levels)
Cdr1as (total output)/Gapdh (normalized levels)
miR-7/U6 (normalized levels)
1.00
0.75
0.50
0.25
0.00
ns
**
*
***
Control
circCdr1as KD
linCdr1as rescue
linCdr1as

Figure 2

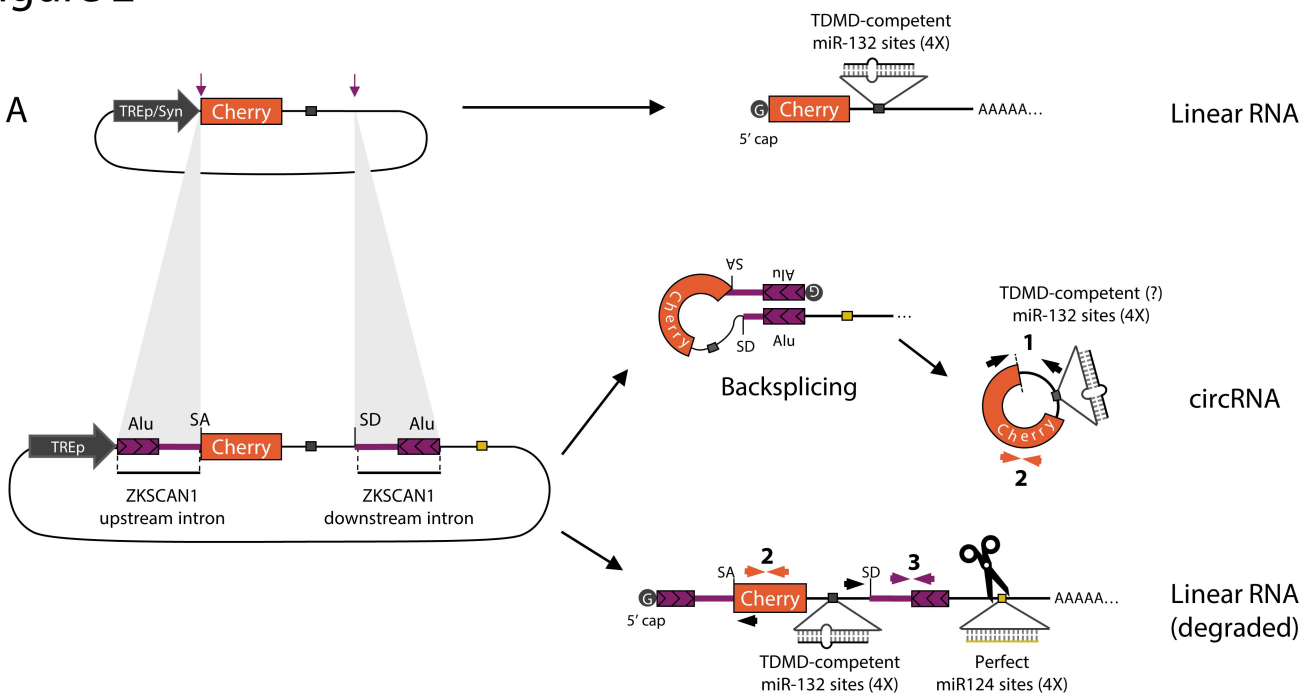
A
TREp/Syn
Cherry
TDMD-competent
miR-132 sites (4X)
Cherry
AAAAA...
5' cap
Linear RNA
SA
Alu
Cherry
SD
Alu
Backsplicing
TDMD-competent (?)
miR-132 sites (4X)
1
2
circRNA
TREp
Alu
SA
Cherry
SD
Alu
ZKSCAN1
upstream intron
ZKSCAN1
downstream intron
2
SA
SD
3
Cherry
AAAAA...
5' cap
TDMD-competent
miR-132 sites (4X)
Perfect
miR124 sites (4X)
Linear RNA
(degraded)

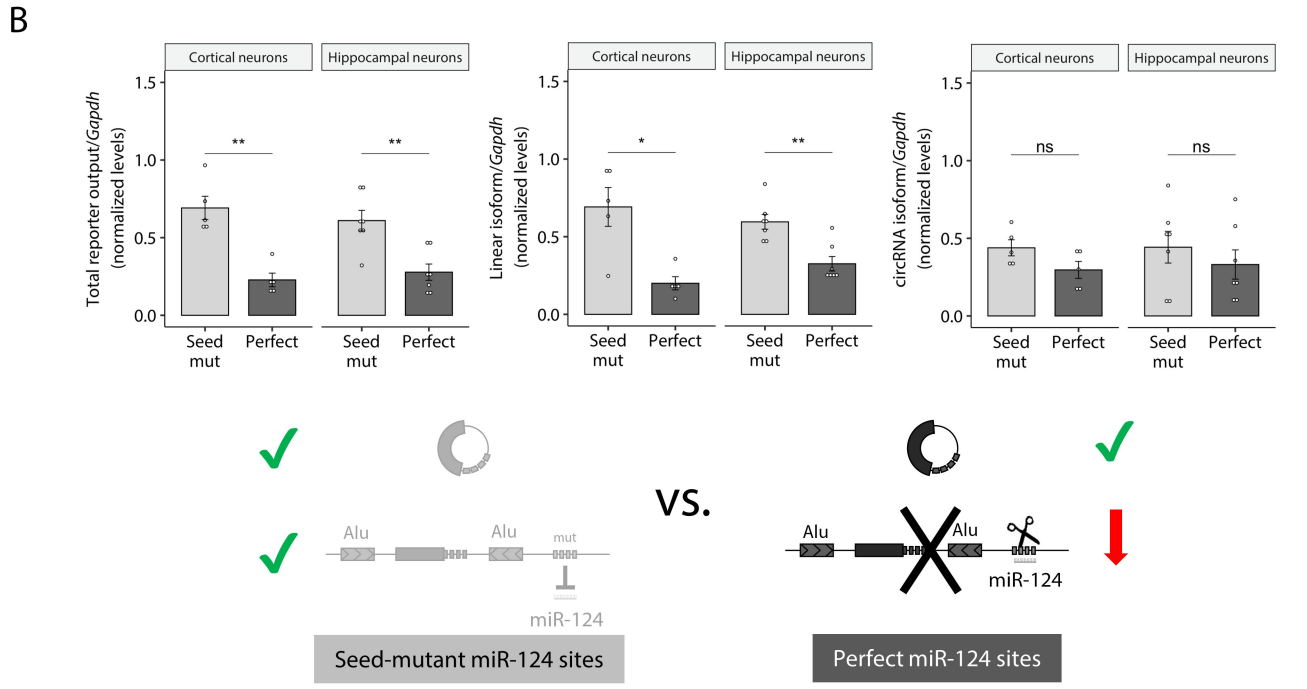
B
Cortical neurons
Hippocampal neurons
Total reporter output/Gapdh
(normalized levels)
Linear isoform/Gapdh
(normalized levels)
circRNA isoform/Gapdh
(normalized levels)
1.5
1.0
0.5
0.0
**
*
ns
Seed mut
Perfect
Alu
mut
miR-124
VS.
Seed-mutant miR-124 sites
Perfect miR-124 sites

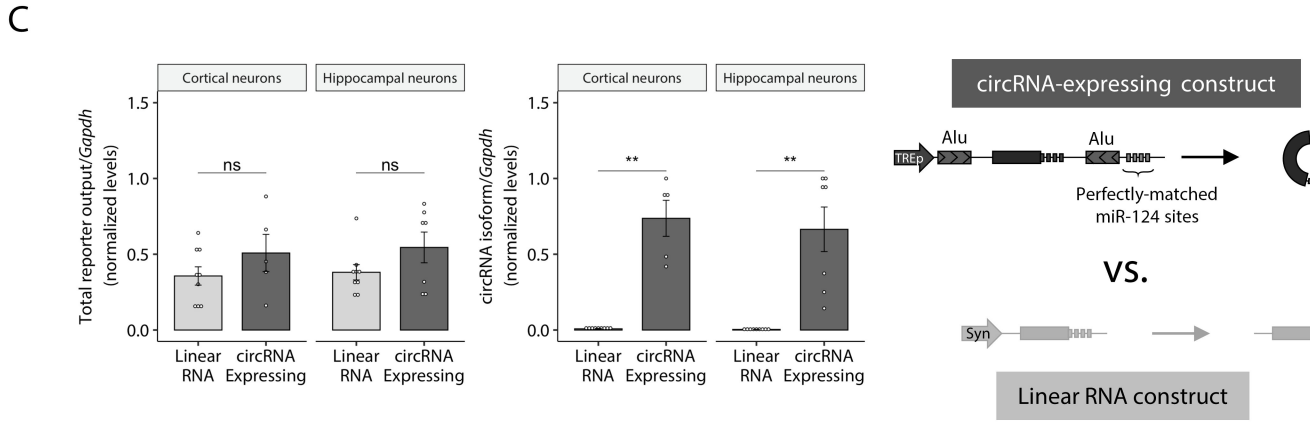
C
Cortical neurons
Hippocampal neurons
Total reporter output/Gapdh
(normalized levels)
circRNA isoform/Gapdh
(normalized levels)
1.5
1.0
0.5
0.0
ns
**
Linear RNA
circRNA Expressing
circRNA-expressing construct
TREp
Alu
Alu
Perfectly-matched
miR-124 sites
VS.
Syn
Linear RNA construct

Figure 3

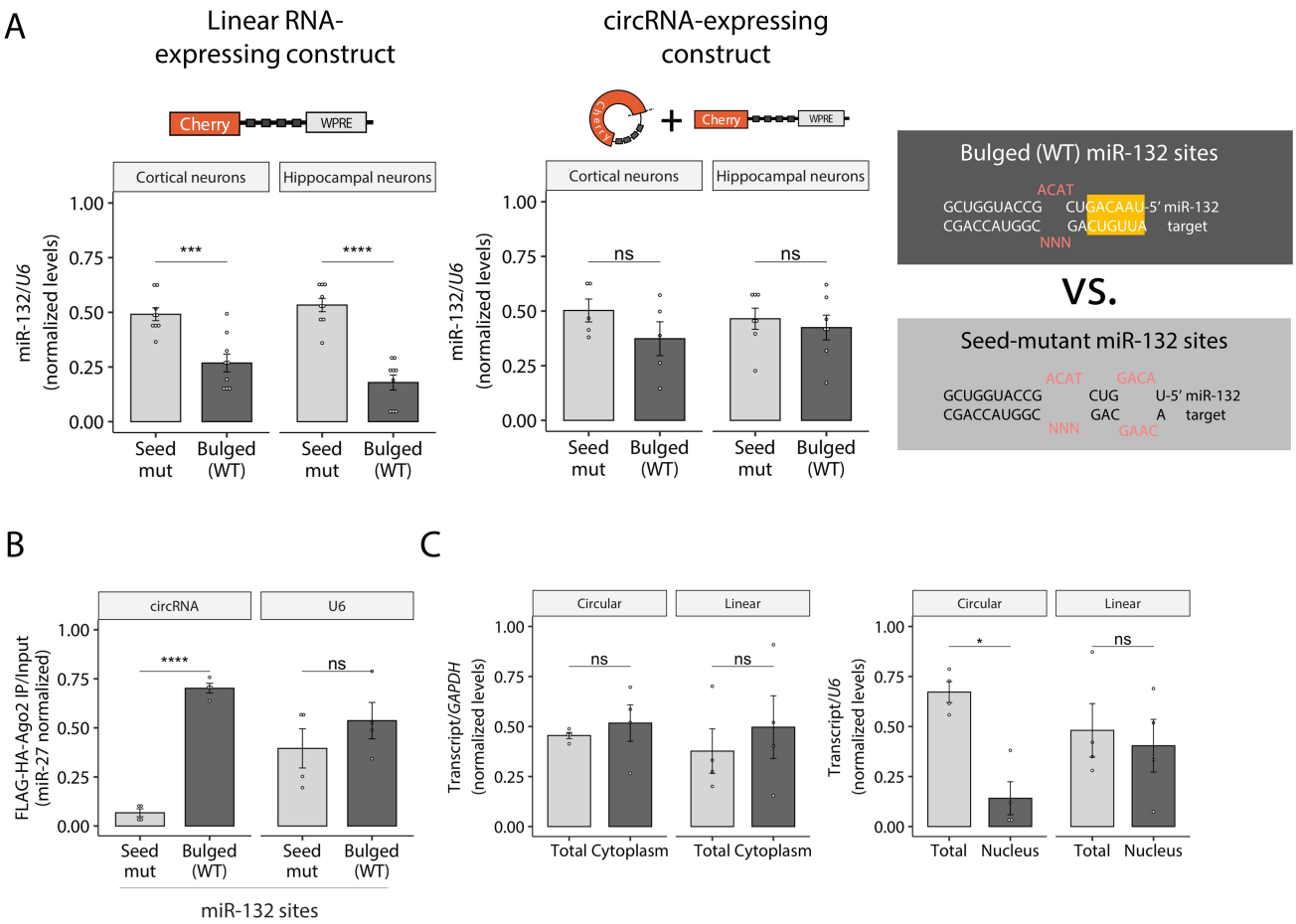
A
Linear RNA-expressing construct
circRNA-expressing construct
Cherry
WPRE
Vector
Cortical neurons
Hippocampal neurons
miR-132/U6 (normalized levels)
1.00
0.75
0.50
0.25
0.00
***
****
ns
Seed mut
Bulged (WT)
Bulged (WT) miR-132 sites
ACAT
GCUGGUACCG
CUGACAAU-5′ miR-132
CGACCAUGGC
GACUGUUA
target
NNN
VS.
Seed-mutant miR-132 sites
ACAT
GACA
GCUGGUACCG
CUG
U-5′ miR-132
CGACCAUGGC
GAC
A
target
NNN
GAAC
B
circRNA
U6
FLAG-HA-Ago2 IP/Input (miR-27 normalized)
miR-132 sites
C
Circular
Linear
Transcript/GAPDH (normalized levels)
Total
Cytoplasm
Transcript/U6 (normalized levels)
Nucleus
*

Figure 4

A

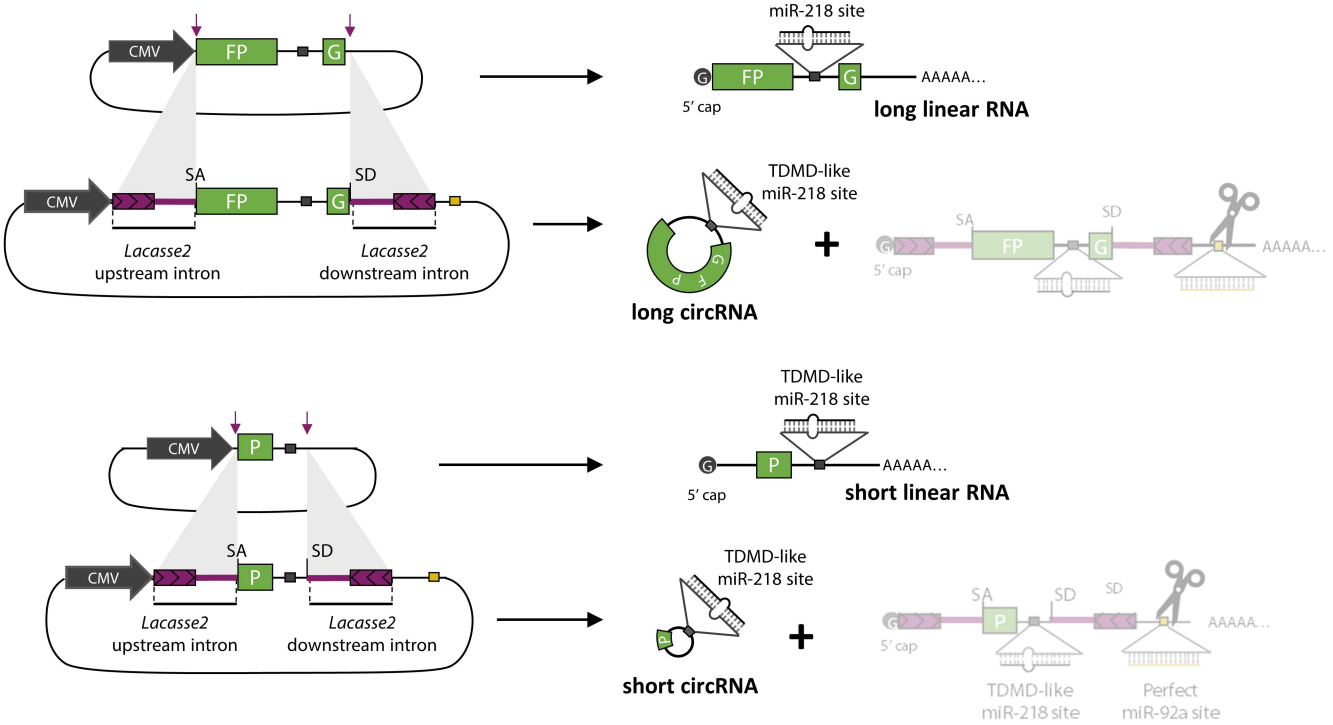
CMV
FP
G
SA
SD
Lacasse2
upstream intron
Lacasse2
downstream intron
TDMD-like
miR-218 site
5′ cap
AAAAA…
long linear RNA
long circRNA
P
short linear RNA
short circRNA
TDMD-like
miR-218 site
Perfect
miR-92a site

B

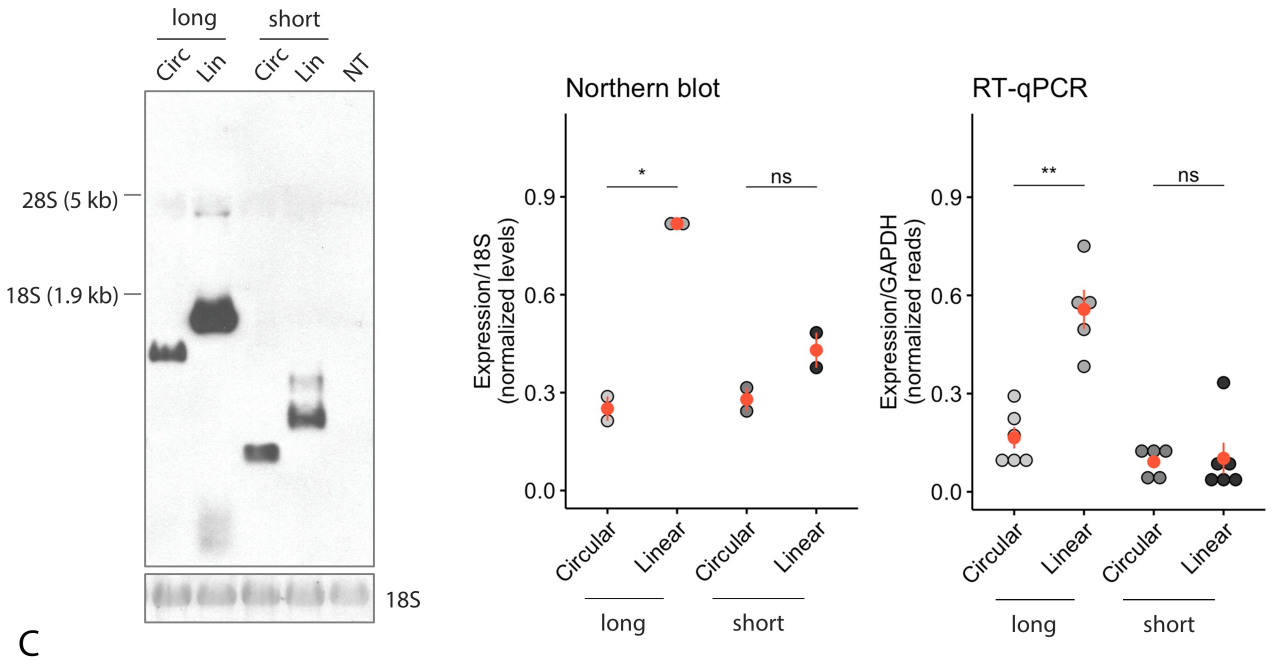
long
short
Circ
Lin
NT
28S (5 kb)
18S (1.9 kb)
18S
Northern blot
RT-qPCR
Expression/18S
(normalized levels)
Expression/GAPDH
(normalized reads)
0.0
0.3
0.6
0.9
*
**
ns
Circular
Linear
long
short

C

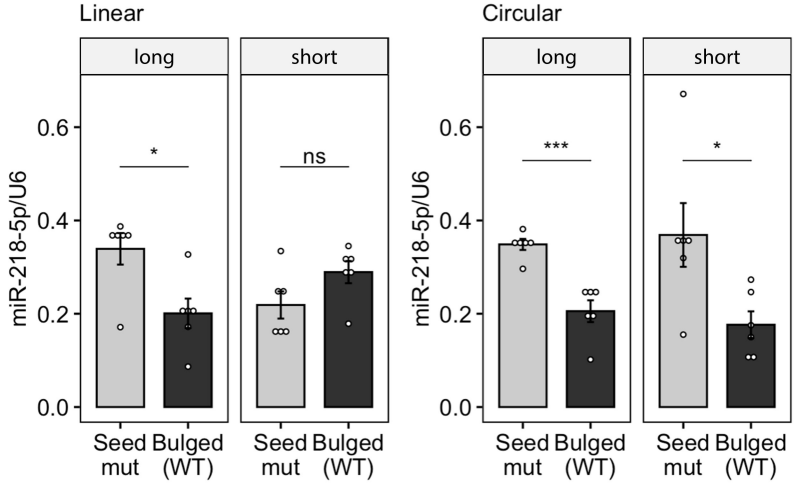
Linear
Circular
long
short
miR-218-5p/U6
0.0
0.2
0.4
0.6
*
***
ns
Seed
mut
Bulged
(WT)

Figure 5

A

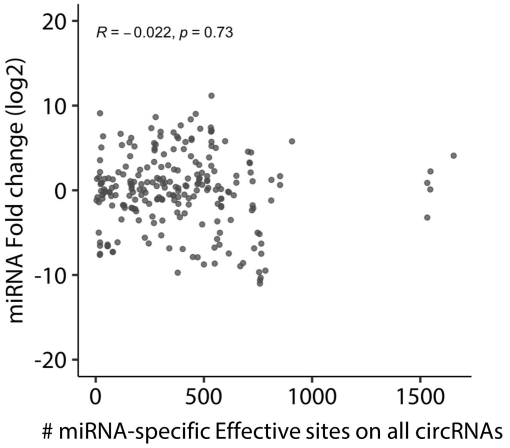

D

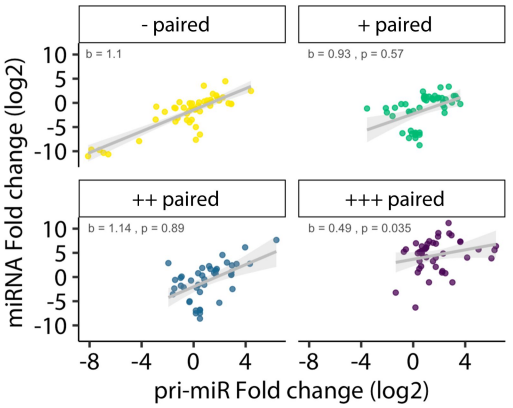

B

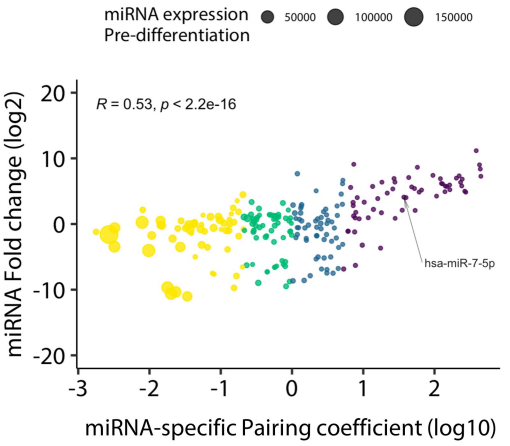

E

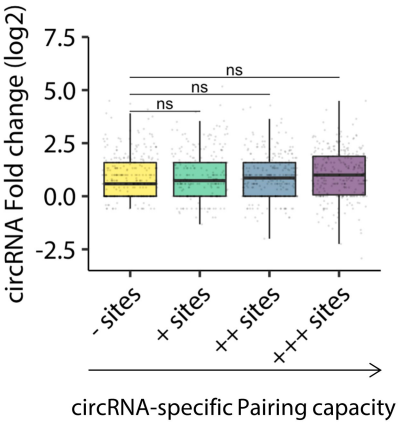

C

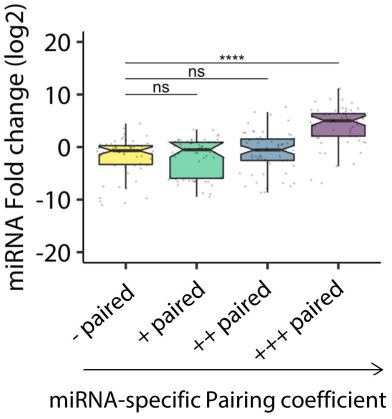

Figure 6

A

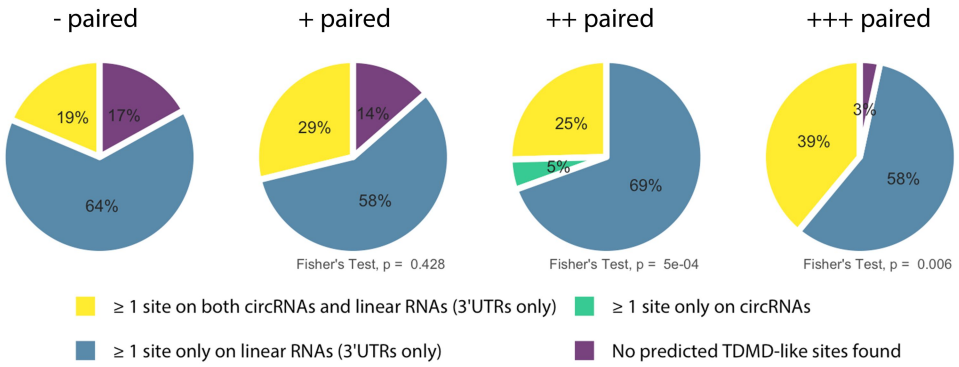
- paired
+ paired
++ paired
+++ paired
19%
17%
64%
29%
14%
58%
25%
5%
69%
39%
3%
58%
Fisher's Test, p = 0.428
Fisher's Test, p = 5e-04
Fisher's Test, p = 0.006
≥ 1 site on both circRNAs and linear RNAs (3'UTRs only)
≥ 1 site only on circRNAs
≥ 1 site only on linear RNAs (3'UTRs only)
No predicted TDMD-like sites found

B

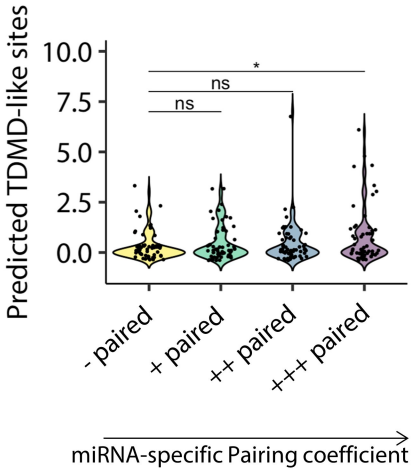
Predicted TDMD-like sites
10.0
7.5
5.0
2.5
0.0
*
ns
ns
- paired
+ paired
++ paired
+++ paired
miRNA-specific Pairing coefficient

Figure EV1

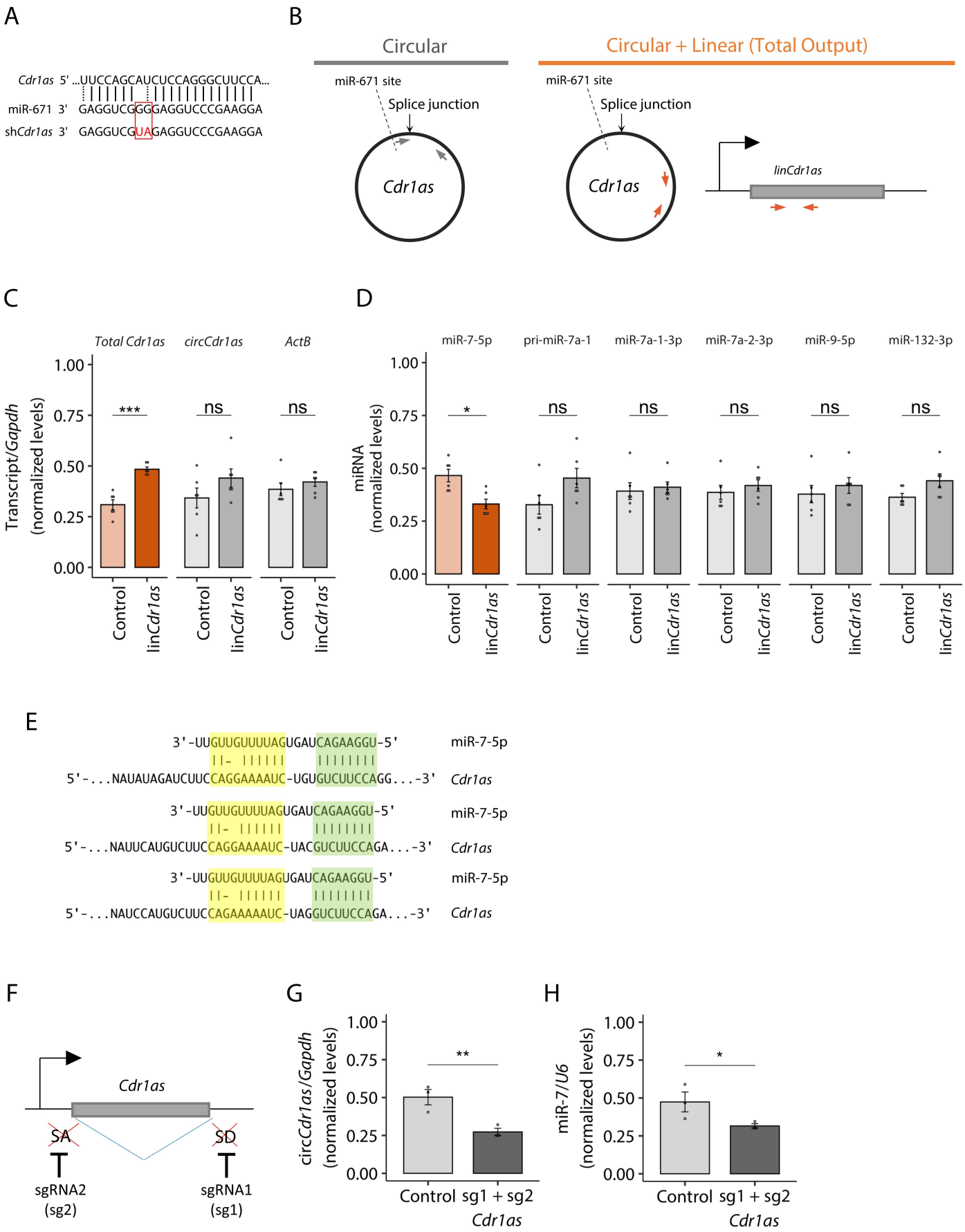
A
Cdr1as 5' ...UUCCAGCAUCUCCAGGGCUUCCA...
miR-671 3' GAGGUCGGGGAGGUCCCGAAGGA
shCdr1as 3' GAGGUCGUAGAGGUCCCGAAGGA
B
Circular
Circular + Linear (Total Output)
miR-671 site
Splice junction
Cdr1as
linCdr1as
C
Total Cdr1as
circCdr1as
ActB
Transcript/Gapdh (normalized levels)
***
ns
Control
linCdr1as
D
miR-7-5p
pri-miR-7a-1
miR-7a-1-3p
miR-7a-2-3p
miR-9-5p
miR-132-3p
miRNA (normalized levels)
*
E
3'-UUGUUGUUUUAGUGAUCAGAAGGU-5' miR-7-5p
5'-...NAUAUAGAUCUUCCAGGAAAAUC-UGUGUCUUCCAGG...-3' Cdr1as
3'-UUGUUGUUUUAGUGAUCAGAAGGU-5' miR-7-5p
5'-...NAUUCAUGUCUUCCAGGAAAAUC-UACGUCUUCCAGA...-3' Cdr1as
3'-UUGUUGUUUUAGUGAUCAGAAGGU-5' miR-7-5p
5'-...NAUCCAUGUCUUCCAGAAAAAUC-UAGGUCUUCCAGA...-3' Cdr1as
F
Cdr1as
SA
SD
sgRNA2 (sg2)
sgRNA1 (sg1)
G
circCdr1as/Gapdh (normalized levels)
**
Control
sg1 + sg2
Cdr1as
H
miR-7/U6 (normalized levels)
*

Figure EV2

A

Construct purpose	miR-132 sites: Type	miR-132 sites: Architecture	miR-124 sites: Type	miR-124 sites: Architecture	Expected RNA topology
circRNA expression (linear RNA-downregulated)	Bulged (WT)	GCUGGUACCG ACAT CUGACAAU-5′ miR-132 CGACCAUGGC NNN GACCUGUUA target	Perfect match	CCGUAAGUGGCGCACGGAAU-5′ miR-124 GGCAUUCACCGCGUGCCUUA target	Circular + low linear leak
	Seed-mut	GCUGGUACCG ACAT CUG GACA U-5′ miR-132 CGACCAUGGC NNN GAC GAAC A target	Perfect match	CCGUAAGUGGCGCACGGAAU-5′ miR-124 GGCAUUCACCGCGUGCCUUA target	Circular + low linear leak
circRNA expression (control)	Bulged (WT)	GCUGGUACCG ACAT CUGACAAU-5′ miR-132 CGACCAUGGC NNN GACCUGUUA target	Seed-mut	CCGUAAGU GGCG CA CGGA AU-5′ miR-124 GGCAUUCA NNN GU CGGA UA target	Circular + high linear leak
	Seed-mut	GCUGGUACCG ACAT CUG GACA U-5′ miR-132 CGACCAUGGC NNN GAC GAAC A target	Seed-mut	CCGUAAGU GGCG CA CGGA AU-5′ miR-124 GGCAUUCA NNN GU CGGA UA target	Circular + high linear leak
linear RNA expression (TDMD inducer)	Bulged (WT)	GCUGGUACCG ACAT CUGACAAU-5′ miR-132 CGACCAUGGC NNN GACCUGUUA target	NA	NA	Linear
	Seed-mut	GCUGGUACCG ACAT CUG GACA U-5′ miR-132 CGACCAUGGC NNN GAC GAAC A target	NA	NA	Linear

B

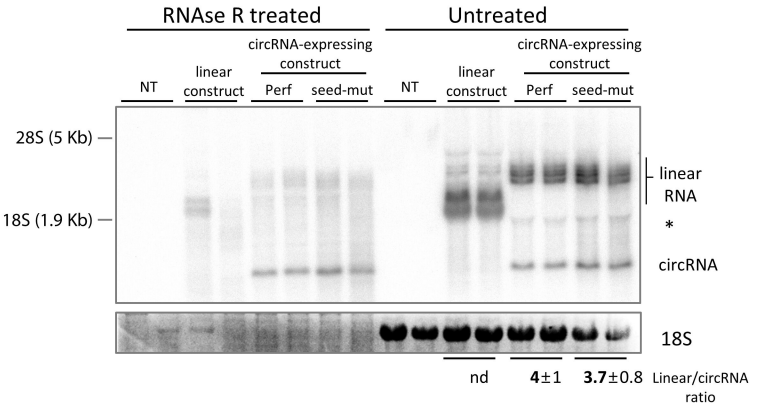

C

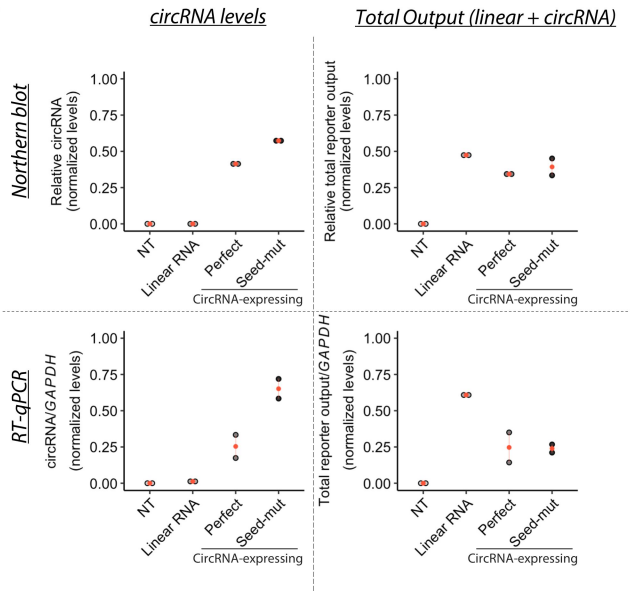

D

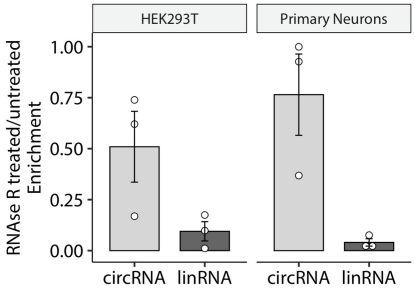

Treatment Tukey p-adj= 0.002 , Cell type Tukey p-adj= 0.482

E

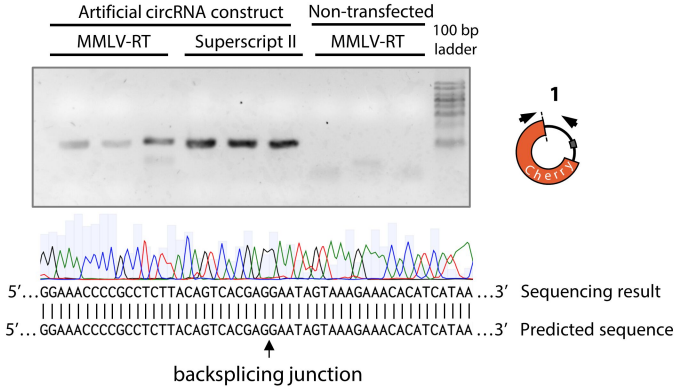

F

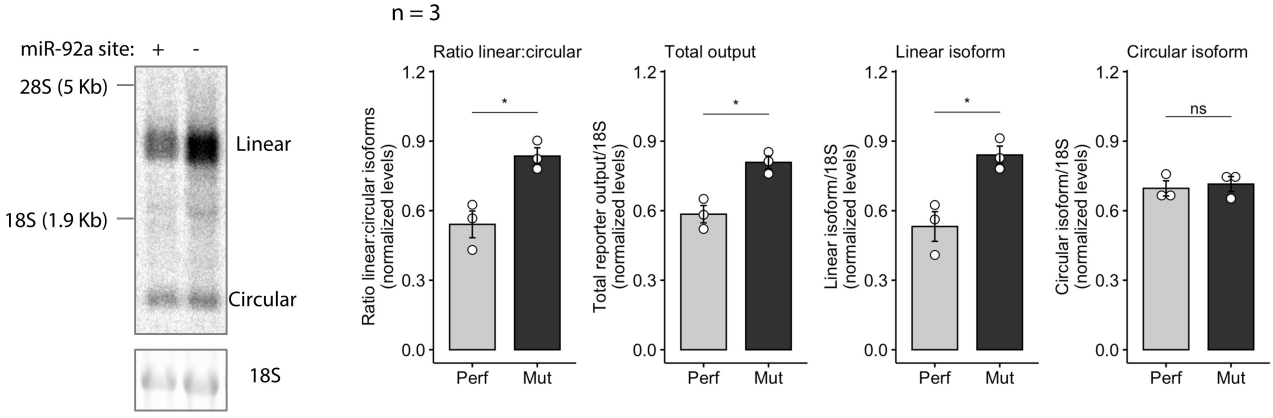

Figure EV3

A

Linear RNA-expressing construct

circRNA-expressing construct

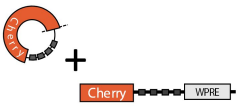

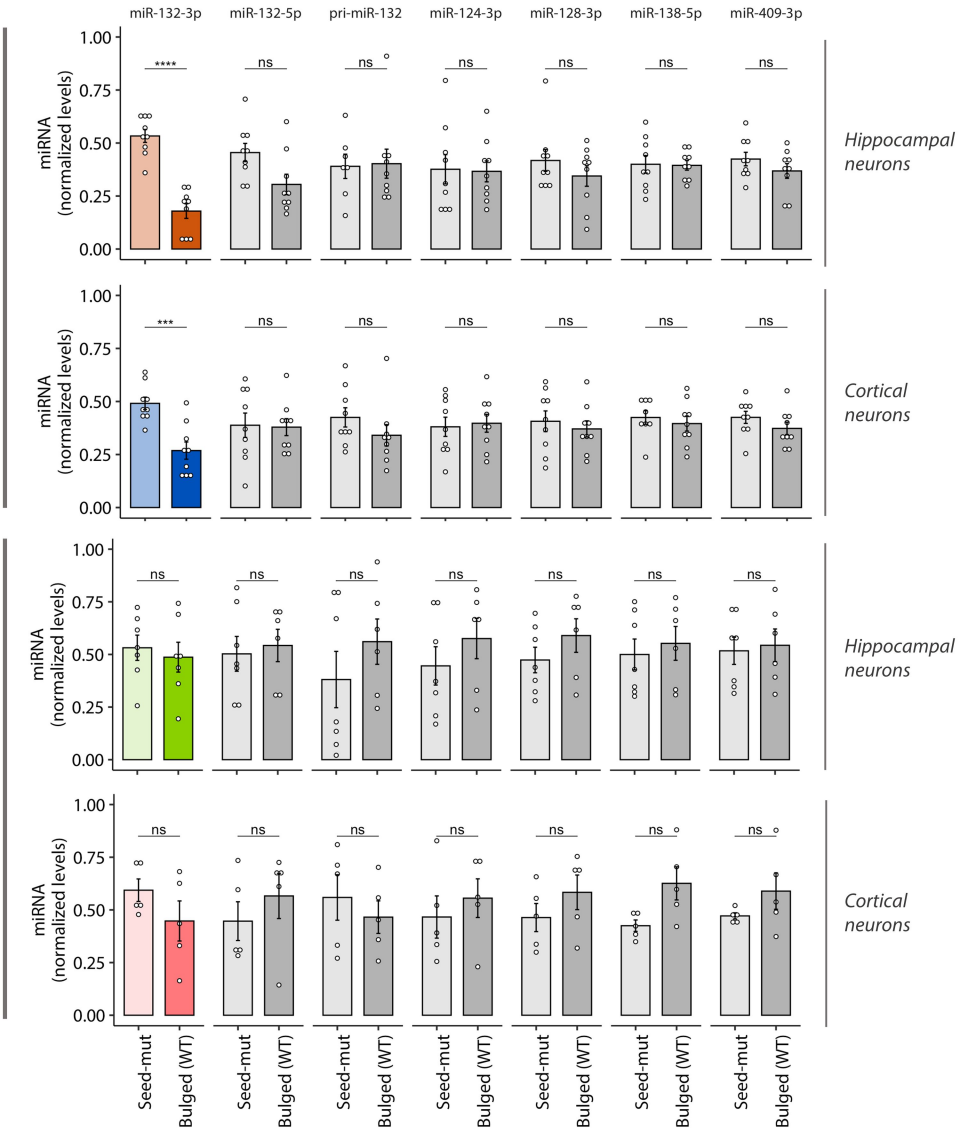

B

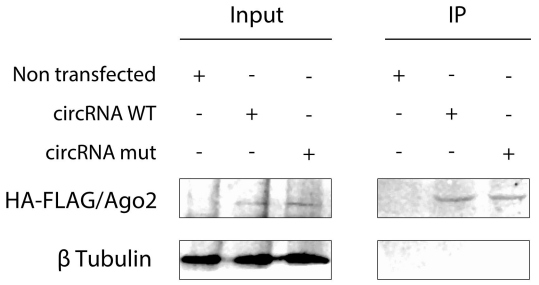

C

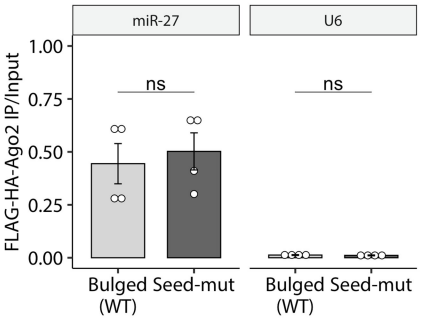

D

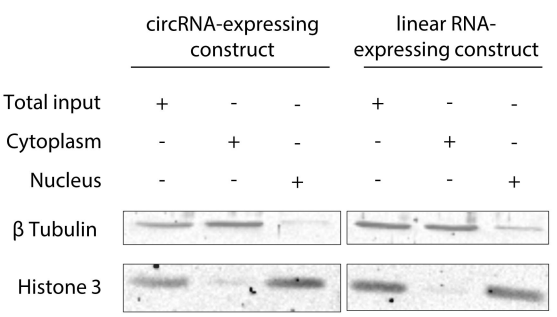

E

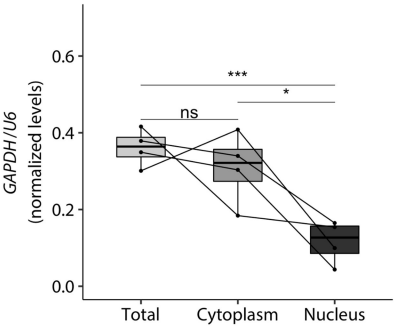

Figure EV4

A

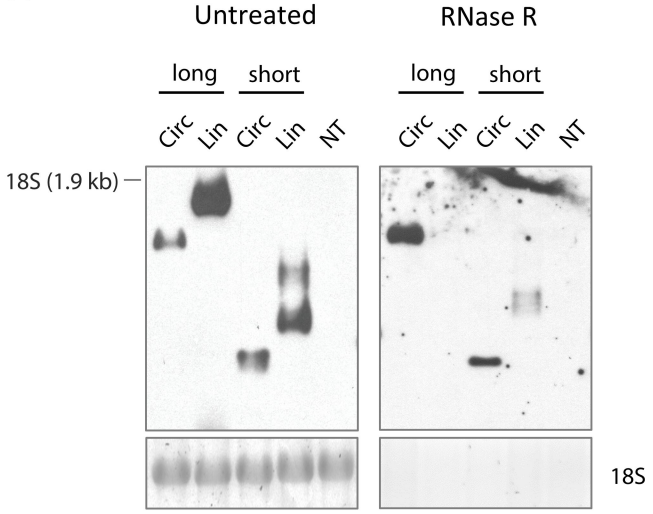

B

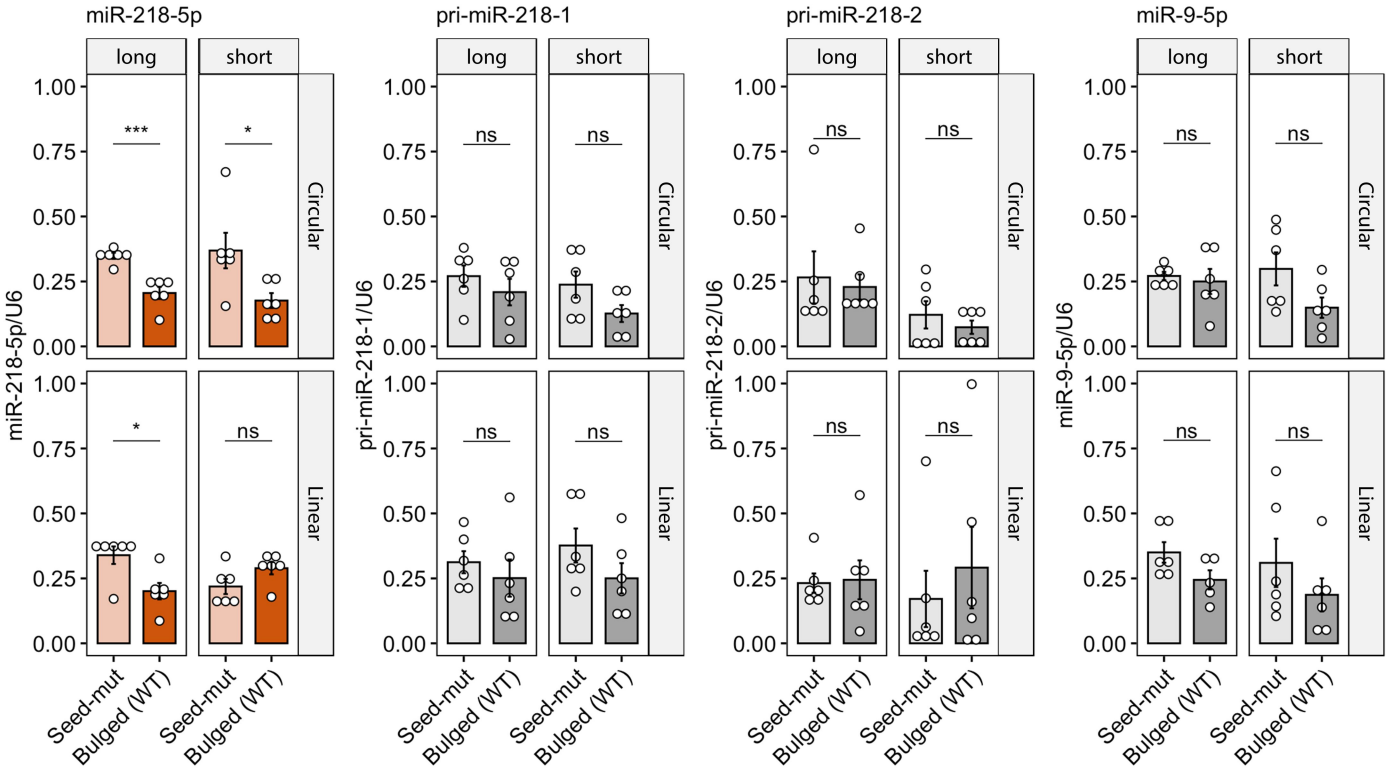

Figure EV5

A

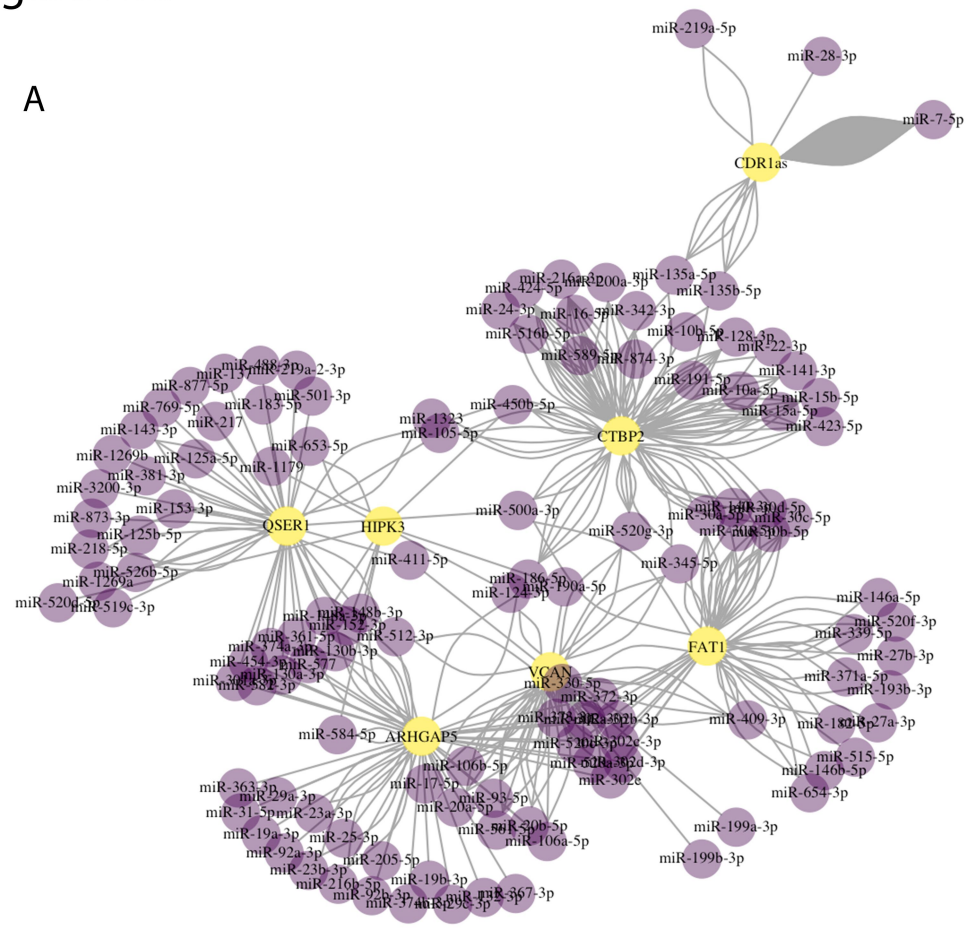

B

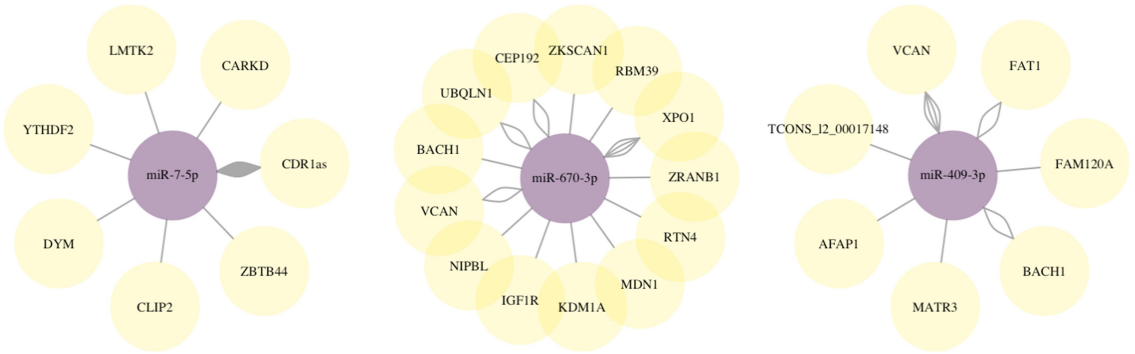

C

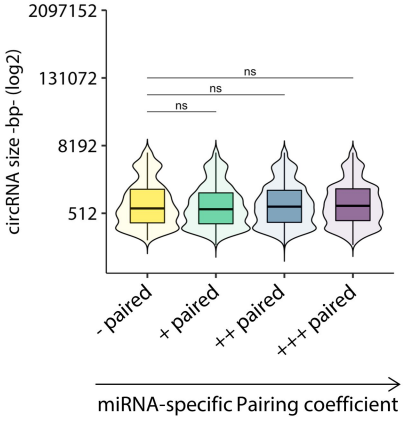

D

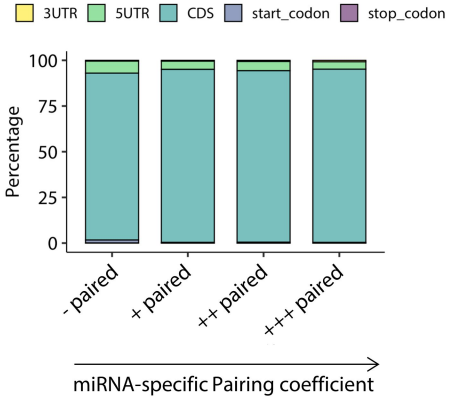

Figure EV6

A

```
          3'-AACGGGAGA---GUUGGGUCGAAAA-5'        miR-320b
             |||-||||        ||||||||
5'-...NUUGGCCCUGCUCUCUGUGACCAUCAGCUUUAGG...-3'   circRTN4 (hsa_circ_0001006)

             3'-CGUUCGGGUCUGGCGUUUUUC-5'         miR-129-5p
               |||||||-    | |||||||
5'-...NGACCAGUACAGCAAGCCU-CCGCACAAAAAACU...-3'   circFNDC3B (hsa_circ_0003692)

          3'-GUGUUUGGUA--AUACACGACGAU-5'         miR-15a-5p
            |||-|-|||  |  ||||||||
5'-...NGGUGCCAGACAGAUCAUGCUUAGUGCUGCUUUA...-3'   circARID1B (hsa_circ_0004019)

            3'-UGUCCGGUAGA-CACAAUAUAA-5'         miR-410-3p
              |||| ||||||     |||||||
 5'-...NUCAAGGCCACAGACCAUCUCUGUUUAUAUAAA...-3'   circRIMS2 (hsa_circ_0005114)

             3'-GGUUGGUUACUUUCUUACGAA-5'         miR-1179
               ||||-||   |  |||||||
5'-...NUUUCAAAUAAGCAACUAA-AUAGAAAUGCUAAU...-3'   circSKIL (hsa_circ_0067938)
```

Examples of predicted TDMD-like sites within circRNAs

B

Circular RNAs

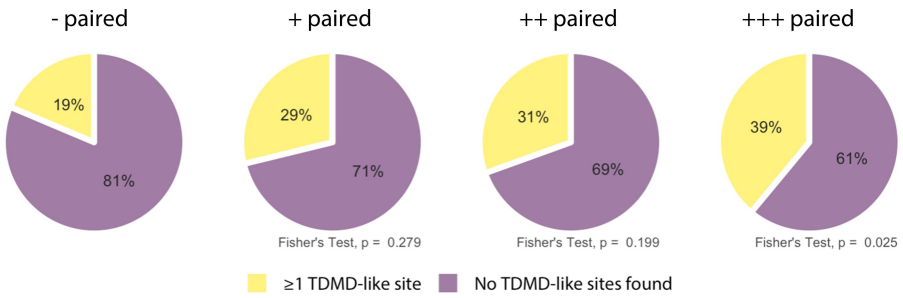

C

Linear RNAs (3' UTR)

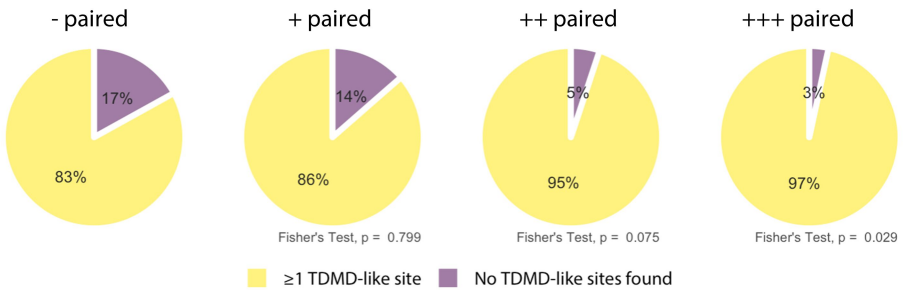

Oligo name/DNA Fragments	Use	Sequence 5'->3'
CiRS7_lin_For1	Linear CDR1as	gggtttccagtggtgccagt
CiRS7_lin_Rev1	Linear CDR1as	ctggatacggcagacaccag
ciRS7_lin_For_BamHI	Linear CDR1as lacking miR-671 site	atccGGATCCgggtttccagtggtgccagt
ciRS7_lin_Rev_SalI	Linear CDR1as lacking miR-671 site	atccGTCGACtgaaggaagacacatgtact
rno-miR-671-gblock_mouse-Cir7-match	shCDR1as	atagccgattagttctcgaggatccgggggcagatttgacc gggcccggctggctggtgaactggcaggccaggaagag ggctccacctctttcgagccgtagagccagggctggtacag cgttgtcgcctcagcaacttggaggggctgctagctcgagc
miR-7_Bulged_sites	Linear TDMD inducer miR-7 bulged	AGCTGTATAAGTAGGCTAGCCGTCACTGATATC CGTCCCACAACAAAATCACCGTCTTCCATATGC AAACCTCACTACAATACAACAAAATCGCTGTCT
miR-7_Mut_sites	Linear TDMD inducer miR-7 mutated	AGCTGTATAAGTAGGCTAGCCGTCACTGATATC CGTCCCACAACAAAATCACCGTACCACATATGC AAACCTCACTACAATACAACAAAATCGCTGTAC
SZSCAN1_Ups_intron	Artificial circRNA	gagcgcagtcgagaggatccttttttttttttgacggagttta cctccacctcctgggttcaagcgtttctcctgcctcagctttcc tagtagagacggggtttcaccatgttggccaggctggtctt ttacaggcgtgagccaccacccccggcctcaggagcgttct ttgtaaaggtacgtactaatgactttttttttatacttcaggaat
SZSCAN1_Downs_intron	Artificial circRNA	taggggaagggaaatgattcaggacgagagtctttgtgct cggtagctcacacctgtaatcccagcactttgggaggctga gtgaaaccttgtctctactaaaaatatgaaaattagccaggc atcacttgaacccaggaggtggaggttgcagtaagccgag aaaaagtcgacaatcaacctctgga
pEGFP-miR_BclI_For	pri-miRs	CATCCTGATCATTTTTCGCAACGGGTTTGCC
GFP_Rev	pri-miRs	CTACTTGTACAGCTCGTCCATGC
TREp_XbaI_For	TRE promoter insert	CTACTtctagataggtttaccactccctatc
TREp_BamHI_Rev	TRE promoter insert	CATCCggatccCTAGGCGCGCCTTAATTAAG
miR-92a_perf oligo F	miR-92a perf site	ggccgcAGTCGAGACAGGCCGGGACAAGTGCA
miR-92a_perf oligo R	miR-92a perf site	cTGTCGACTATTGCACTTGTCCCGGCCTGTCTCC
miR-92a_mut oligo F	miR-92a mut site	ggccgcAGTCGAGACAGGCCGGGATGGTAATCT
miR-92a_mut oligo R	miR-92a mut site	CTTGTCGACTAGATTACCATCCCGGCCTGTCTC
miR-218-5p_TDMD site_Template	miR-218 TDMD site template	CACCCTAAAATGCTTCACATGGTTAAAAACAAC
miR-218-5p_TDMD site MUT_Template	miR-218 mut site template	CACCCTAAAATGCTTCAGTACCAAAAAAAGTAC
miR-218-5p_TDMD site_For	miR-218 cloning primer for with BsrGI	actgctgtacaagtaaCAGTCACCCTAAAATGCTTC
miR-218-5p_TDMD site_Rev	miR-218 cloning primer rev with BsrGI	tcatgtgtacaCCTTGCTGTAGGATTCAAAA
GFP Split_NheI_For	Producing the linear control for split-GF	CATCAGCTAGCgagcgcaccatcttcttcaa
GFP Split_XbaI_Rev	Producing the linear control for split-GF	catcgTCTAGActggacgtagccttcgggca
GFP_AgeI_For	Shorter circRNA	ggtcagACCGGTagaacggcatcaaggtgaac
IRES_SacII_Rev	Shorter circRNA	cgttgtCCGCGGcgtcgactgcagaattcaga
GFP_NheI_For	Shorter linear control	gtgcatGCTAGCagaacggcatcaaggtgaac
IRES_XbaI_Rev	Shorter linear control	cctatgTCTAGAcgtcgactgcagaattcaga
miR-92a_perf g-block	g-block for miR-92a perf site addition to the ZKSCAN1 circRNA expressing constructs	CTGTCTTAAAAAAAAAAAAAGTCGAGACAGGCC CGGGACAAGTGCAATATAACTTTTAACACAAC TAAAACAGGCCGGGACAAGTGCAATAGTCGAC
miR-92a_mut g-block	g-block for miR-92a mut site addition to the ZKSCAN1 circRNA expressing constructs	CTGTCTTAAAAAAAAAAAAAGTCGAGACAGGCC GGGATGGTAATCTATAACTTTTAACACAACAA AACAGGCCGGGAGCGTAATCTAGTCGACAATC
sgCiRS7-1_For	sgRNA to mutate CDR1as splice sites	CACCGATGAAACAACTTTCAATACC
sgCiRS7-1_Rev	sgRNA to mutate CDR1as splice sites	AAACGGTATTGAAAGTTGTTTCATC
sgCiRS7-2_For	sgRNA to mutate CDR1as splice sites	CACCGATGATGTTTCCAATATCTAG
sgCiRS7-2_Rev	sgRNA to mutate CDR1as splice sites	AAACCTAGATATTGGAAACATCATC

:ggcaggcatcagcagagggctgcttctacaacgctgactacctggcagccc
gaggaagccctggagatgctggaggtgatggatgttttcctccggtgttcag
gaagttctccctgagggactgcagcccccggctcagtgaggaactgtaccac
ctttggagaatat

GCTCGAACAACAAAATCTCCGTCTTCCATACAATTTAAAACC
CCCGTCCTCTCTCTTTACAACAAAATCTACGTCTTCCACTTGC
TTCCAGTCGACAATCAACCTCTGGA

GCTCGAACAACAAAATCTCCGTACCACATACAATTTAAAACC
CCCGTCCTCTCTCTTTACAACAAAATCTACGTACCACACTTGC
CCACAGTCGACAATCAACCTCTGGA

acttcttgtctcccaggtaggaagtgcagtggcgtaatctcggctcactacaa
:gagtagctgggattacaggcgcctgccaccatgccctgctgacttttgtatttt
gaactcctgaccgcaggcgattggcctgcctcggcctcccaaagtgctgaga
tgatagtgcctcgatgtgctgcctcctataaagtgttagcagcacagatcacttt
tagtaaagaaacacatcataaaacctcccaccggtcgccaccatggtga

gctgagtgcctgtgatgaagaagcatgttagtgaaaagaattaggctcggca
ggcgggcagatcacttgaggtcaggagtttgagaccagcctggccaacatg
atggtggcacattcctgtaatcccagctactcgggaggctgaggcaggaga
gatcgtaccactgtgctctagccttggtgacagagcgagactgtcttaaaaaaa

ATAGTCGACAgggcc
GACTgc
TAGTCGACAAgggcc
GACTgc
GCACAATTTTGAATCCTACAGC
CGTCAATTTTGAATCCTACAGC

CGGGACAAGTGCAATATACAACATTTACATTTAACAACAGGC
AAAAACAGGCCGGGACAAGTGCAATATTATTCTTACTTTAGT
CAATCAACCTCTGGAttacaaaatt
CGGGATCGTAATCTATACAACATTTACATTTAACAACAGGCC
AAACAGGCCGGGACGGTAATCTATTATTCTTACTTTAGTTAA
CAACCTCTGGATTACAAAATT

Custom-made qPCR Mix	**µL per Reaction**
*10X Reaction Buffer **	2.5
MgCl2 25 mM	4
Triton x-100 10%	0.06
dNTP mix 10mM	0.5
Glycerol 60%	1.67
DMSO 100%	0.25
Betaine 5M	1.25
*Taq Polymerase (5 U/µL) ***	0.1
*SYBR Green (1/90)****	0.03
Primer Forward 10 µM	0.5
Primers Reverse 10 µM	0.5
H20	8.64
cDNA	5
Final volume	25

* 10X TAS reaction buffer from INBIO Highway

** Taq Polymerase from INBIO Highway

***SYBR Green (Sigma S9430).

***qPCR program:* 94°C-3′; (94°C-15′′; 60°C-15′′; 72°C-25′′) 40x, melting curve. All reactions were run in either an ABI Qua

antstudio 3 or an ABI StepOnePlus.

qPCR

Oligo name	Comments	Sequence 5'->3'
circ_Cdr1as F	Circular CDR1as divergent	cctacaactgcccagtgtctc
circ_Cdr1as R	Circular CDR1as divergent	ggtactggcaccactggaaa
TO_Cdr1as F	Circular + linear CDR1as (total output)	tgtgtcttccttcacctccag
TO_Cdr1as R	Circular + linear CDR1as (total output)	ctggatacggcagacaccag
qWPRE_For	Linear CDR1as/artificial linRNA control exclusively	actgtgtttgctgacgcaac
qWPRE_Rev	Linear CDR1as/artificial linRNA control exclusively	caacaccacggaattgtcag
Artificial_circ F	Circular artificial circRNA divergent	TACAAGTAAAGCGGCCGCGTCG
Artificial_circ R	Circular artificial circRNA divergent	CTCGCCCTTGCTCACCATGGTG
Artificial_circ_TO F	Circular + linear artificial circRNA (Total output)	gtggaacagtacgaacgcgcc
Artificial_circ_TO R	Circular + linear artificial circRNA (Total output)	CTACTTGTACATATGATTAGTGGTTTAAA
Artificial_circ_lin F	Linear artificial leak exclusively (combined with Artificial_circ_For)	TGAGCTACCGTGCCGAGCCTAA
mmu_pri-miR-132 F	pri-miR-132 qPCR (only mouse)	GCACGCCTGTTCAAGGTCCCTG
mmu_pri-miR-132 R	pri-miR-132 qPCR (mouse and rat)	CCCCGCCTCCTCTTGCTCTGTA
mmu_pri-miR-7 F	pri-miR-7 qPCR (only mouse)	GCCTGTAGAAAATGTAGAAGAGAC
mmu_pri-miR-7 R	pri-miR-7 qpCR (mouse and rat)	TATGGCAGACTGTGATTTGTTG
hsa-miR-132-3p STEM	Conserved in rat and mouse	GTCTCCTCTGGTGCAGGGTCCGAGGTAT
hsa-miR-132-3p Fw	Conserved in rat and mouse	GGCGGUAACAGUCUACAGCC
hsa-miR-9-5p Stem	Conserved in rat and mouse	GTCTCCTCTGGTGCAGGGTCCGAGGTAT
hsa-miR-9-5p Fw	Conserved in rat and mouse	GGCGGUCUUUGGUUAUCUAGC
hsa-miR-7-5p Stem	Conserved in rat and mouse	GTCTCCTCTGGTGCAGGGTCCGAGGTAT
hsa-miR-7-5p Fw	Conserved in rat and mouse	GGCGGUGGAAGACUAGUGAUUU
mmu-miR-7-1-3p Stem	Conserved in human	GTCTCCTCTGGTGCAGGGTCCGAGGTAT
mmu-miR-7-1-3p Fw	Conserved in human	GGCGGCAACAAATCACAGTC
rno-miR-7a-2-3p Stem	Conserved in mouse	GTCTCCTCTGGTGCAGGGTCCGAGGTAT
rno-miR-7a-2-3p Fw	Conserved in mouse	GGCGGCAACAAGTCCCAGTC
miR Rev Universal	-	TGGTGCAGGGTCCGAGGTATT
ActB F	Conserved in rat and mouse	CTAAGGCCAACCGTGAAAAG
ActB R	Conserved in rat and mouse	ACCAGAGGCATACAGGGACA
Klf4f	miR-7 Target	aaaagaacagccaccacac
Klf4r	miR-7 Target	tcccagtcacagtggtaagg
Egr3f	miR-7 Target	cgcgctcaacctcttctc
Egr3r	miR-7 Target	attgggcttctcgttggtc
Irs2f	miR-7 Target	gagtgtgtgggggtccag
Irs2r	miR-7 Target	aatgtagaattgctcccgttg
Nr4a3f	miR-7 Target	tgcctgtcagcactgagtatg
Nr4a3r	miR-7 Target	agagcctgtcccttcctgt

Northern Probes

Oligo name	Comments	Sequence 5'->3'
GFP (-41 to -60 nt from stop)	Biotin label at the 5'end	gtcacgaactccagcaggac

AAT

TCGCACCAGAGGAGACCGACCA

TCGCACCAGAGGAGACTCATAC

TCGCACCAGAGGAGACAACAAC

TCGCACCAGAGGAGACTATGGC

TCGCACCAGAGGAGACTGTGGC